Dynamics associated with a quasiperiodically forced Morse oscillator: Application to molecular dissociation

Darin Beigie
Department of Physics, California Institute of Technology, Pasadena, California 91125

Stephen Wiggins
Department of Applied Mechanics, California Institute of Technology, Pasadena, California 91125
(Received 19 June 1991)

The dynamics associated with a quasiperiodically forced Morse oscillator is studied as a classical model for molecular dissociation under external quasiperiodic electromagnetic forcing. The forcing entails destruction of phase-space barriers, allowing escape from bounded to unbounded motion. In contrast to the ubiquitous Poincaré map reduction of a periodically forced system, we derive a sequence of nonautonomous maps from the quasiperiodically forced system. We obtain a global picture of the dynamics, i.e., of *transport in phase space,* using a sequence of time-dependent two-dimensional lobe structures derived from the invariant homoclinic tangle of a persisting invariant saddle-type torus in a Poincaré section of an associated autonomous system phase space. Transport is specified in terms of two-dimensional lobes mapping from one to another within the sequence of lobe structures, and this provides the framework for studying basic features of molecular dissociation in the context of classical phase-space trajectories. We obtain a precise criterion for discerning between bounded and unbounded motion in the context of the *forced* problem. We identify and measure analytically the *flux* associated with the transition between bounded and unbounded motion, and study dissociation rates for a variety of initial phase-space ensembles, such as an even or weighted distribution of points in phase space, or a distribution on a particular level set of the unperturbed Hamiltonian (corresponding to a quantum state). A *double-phase-slice* sampling method allows exact numerical computation of dissociation rates. We compare single- and two-frequency forcing. Infinite-time average flux is maximal in a particular single-frequency limit; however, lobe penetration of the level sets of the unperturbed Hamiltonian can be maximal in the two-frequency case. The variation of lobe areas in the two-frequency problem gives one added freedom to enhance or diminish aspects of phase-space transport on finite time scales for a fixed infinite-time average flux, and for both types of forcing the geometry of lobes is relevant. The chaotic nature of the dynamics is understood in terms of a *traveling horseshoe map sequence.*

PACS number(s): 33.80.Gj, 05.45.+b

I. INTRODUCTION

Periodically forced nonlinear oscillators and coupled nonlinear oscillators have been studied as models for a variety of atomic and molecular phenomena, such as multiphoton ionization of excited atoms [1–7], multiphoton dissociation of diatomic and polyatomic molecules [8–14], and unimolecular and bimolecular reactions [15–21]. In this paper we consider a quasiperiodically forced Morse oscillator as a classical model of molecular dissociation under external quasiperiodic electromagnetic forcing. The unforced Morse oscillator is a one degree-of-freedom Hamiltonian system whose unperturbed phase portrait contains a separatrix that divides bounded and unbounded motion, and the use of dynamical systems theory in the ubiquitous case of *periodically* forcing such a system is by now well established, indeed commonplace, being employed in a variety of physical problems [7,22–27]. The immense popularity of, and indeed almost exclusive focus on, this type of forcing is related to the fact that, by time-periodic sampling of phase-space trajectories, the study reduces to that of a two-dimensional Poincaré map, so that one is fully armed with all the tools and paradigms from dynamical systems theory associated with *two-dimensional maps* (to be described momentarily). It is in this context that, without resorting to statistics, one can answer basic questions about molecular dissociation in the context of phase-space trajectories, such as the following.

(i) Is there a precise criterion for discerning between bounded and unbounded motion in the context of the *forced, nonintegrable* problem and, if so, is there a practical way to determine this criterion and study its properties?

(ii) Can one identify in a nonstatistical manner which points in phase space undergo the transition between bounded and unbounded motion, corresponding to molecular dissociation, and at what time these points make the transition?

(iii) Can one identify and measure a *flux* associated with the transition between bounded and unbounded motion? More ambitiously, is there a way to quantify dissociation rates for a variety of possible initial phase-space ensembles, such as an even or weighted distribution of points in phase space, or a distribution on a particular level set of the unperturbed Hamiltonian (corresponding

to a quantum state)? Can one control these rates in any way?

(iv) How does one establish the existence of a chaotic response to the forcing and appreciate its significance?

Our goal is to address these questions in the context of forcing with more complicated time dependences than periodic, focusing for concreteness on quasiperiodic (two-frequency) forcing. There is obvious motivation to relax the restriction to the special case of periodic forcing, for it allows one to study more complicated scenarios: for example, one can study forcing by two lasers at different frequencies and compare with forcing by one. The basic difficulty in the extension past periodic forcing is that, for any choice of discrete time sampling of phase-space trajectories, the study does not in general reduce to a two-dimensional map, but to a *sequence* of two-dimensional maps. Hence, all the conceptual machinery and mathematical tools associated with iterates of a single two-dimensional map, such as horseshoe maps, KAM (Kolmogorov-Arnold-Moser) tori, fixed partial barriers, turnstiles, and so forth, do not apply here. In extending the analysis to sequences of maps, we will in addition to questions (i)–(iv) want to ask the following.

(v) Is there a way to compare the relative effects of each frequency on questions (i)–(iv)?

(vi) Is there a way to compare flux and dissociation rates between single- and multiple-frequency systems, and say which is "better" or "worse"?

(vii) Do more complicated forcing time dependences lead to new features in molecular dissociation, and can one exploit these features?

(viii) What is "chaos" in the context of a *sequence* of maps, where the horseshoe map paradigm does not apply, and how does multiple-frequency forcing affect chaos?

Before outlining how we will proceed to answer these questions for quasiperiodic forcing, let us first briefly summarize the approach associated with periodic forcing. Periodic forcing destroys the separatrix, which acted as a *complete barrier* between bounded and unbounded motion in the unforced case, and this destruction entails a mechanism for *escape* from bounded to unbounded motion, corresponding to molecular dissociation. Dynamical systems theory offers a conceptual framework for studying dissociation and answering questions (i) to (iv) by establishing *phase-space structure* and using this structure to study *phase-space transport* (what we mean by this and the brief description that follows should be made quite apparent in the systematic study of quasiperiodic forcing to follow). This structure is provided by a set of invariant manifolds of the associated Poincaré map (these manifolds are global stable and unstable manifolds of a persisting saddle-type fixed point of the Poincaré map). One can use these manifolds to precisely define *partial barriers* in phase space between regions of bounded and unbounded motion, and to identify the *turnstile lobes* that are the gateways for transport from one region to another. These barriers and turnstiles are *fixed* in the Poincaré section. Having identified the turnstiles, one can then study flux from bounded to unbounded motion, and dissociation rates. Flux is determined by measuring the turnstile lobe area, which can be done by an approximate analytical method using Melnikov theory, or by exact numerical computation of the turnstile lobe boundaries. For dissociation rates associated with an initial even distribution of points in phase space, a popular approximation in chemical kinetics studies involves a Markov-model approach [15,16,21,28,29], but the deficiencies of such an approximation will be discussed later. An exact method for calculating dissociation rates, for a variety of initial distributions, involves studying the topology of intersections of preimages of the turnstile lobes with the appropriate geometrical objects (depending on the problem at hand), such as the turnstiles themselves, or the level sets of the unperturbed Hamiltonian. Lastly, Melnikov theory allows one to study when the oscillator will respond chaotically to the forcing.

For extension to quasiperiodic forcing, the basic question we need to address, before addressing the other eight questions is: since a sequence of maps is needed to deal with more complicated forcing time dependences, what is the phase-space structure associated with a sequence of maps, and how is this structure used to study phase-space transport in such a way as to quantify molecular dissociation? Our approach to answering this question will be to first rewrite the forced system in autonomous form in order to obtain a set of invariant manifolds in a Poincaré section of the enlarged phase space (these manifolds are the global stable and unstable manifolds of a persisting invariant saddle-type 1-*torus* of the Poincaré map). The geometric structure provided in this autonomous setting is then related back to the original nonautonomous sequence of maps: one understands the sequence of maps in terms of the Poincaré map acting on a sequence of two-dimensional *slices* of the higher-dimensional Poincaré section. The intersection of the time-dependent slices with the invariant structures in the autonomous setting defines a *sequence of time-dependent structures* for the sequence of maps. These structures then generate a sequence of time-dependent partial barriers between bounded and unbounded motion, and a sequence of time-dependent turnstile lobes. The basic feature of the analysis is thus the variation with sample time of the relevant geometrical structure: to understand bounded and unbounded motion under quasiperiodic forcing, one *must* deal with time-dependent constructs, and the fact that these constructs are derived from an invariant structure embedded in an enlarged phase space allows one to embrace the more complicated transport issues associated with sequences of maps.

The paper is organized as follows. In Sec. II we define the sequence of maps associated with the quasiperiodically forced Morse oscillator, and then study the geometrical structure associated with the oscillator recast in the autonomous form. The geometrical possibilities are far richer than for periodic forcing, and in Sec. III we introduce and calculate the quasiperiodic Melnikov function and use the function to study the geometry. Intimately related to the Melnikov function are the frequency-dependent *relative scaling factors,* which provide a measure of the relative effect of each forcing frequency on the

geometry. In Sec. IV we derive the *sequence* of two-dimensional time-dependent phase-space structures from the invariant one in the enlarged phase space, and use this to define the sequence of partial barriers between bounded and unbounded motion and the sequence of turnstiles as the gateway for transport between these regions. Section V, the bulk of the paper, focuses on quantifying transport in phase space in order to study molecular dissociation. We first describe and use a *double-phase-slice* sampling method to numerically compute the partial barriers and the turnstile boundaries for an arbitrary time sample, which provides the framework for *exact* computation of transport quantities under the sequence of maps. We then describe and quantity *flux* associated with *escape* to unbounded motion (i.e., molecular dissociation) and *capture* into bounded motion: relevant measures include instantaneous flux, finite-time average flux, and infinite-time average flux associated with both escape and capture, and the quasiperiodic Melnikov function affords an approximate analytical expression for all these measures, good for small forcing. Note that in contrast to the case of periodic forcing, these measures of flux are in general different, with the sole exception that infinite-time average flux associated with escape and capture are identical. It is found that the infinite-time average of the flux is maximal in the single-frequency limit associated with the larger relative scaling factor (i.e., in this context single-frequency forcing is the best one can do). Though flux is a popular concept in molecular dissociation problems, we assert its limitations and consider several other transport features that help describe dissociation. In particular, we address the question of dissociation probability for an even or weighted initial distribution of points in phase space, which has relevance to the dissociation of an ensemble of excited diatomic molecules. As mentioned before, a popular approach to this dissociation problem in the context of maps employs a Markov model; we extend such an approach to sequences of maps, and then stress the deficiencies of such an approach, and the need to consider the geometry associated with the intersections of preimages of the turnstile lobes with the turnstiles. This lobe intersection analysis, which provides the basis for *exact* computation of the dissociation rates, extends from maps to sequences of maps in a straightforward manner. The main new feature associated with sequences of maps is the *variation of lobe areas:* this variation gives one added freedom to alter finite-time transport quantities for a fixed infinite-time average flux. As an additional dissociation problem, we discuss penetration of the unperturbed energy levels by the turnstiles and their preimages (which has relevance to forcing a system prepared in a particular quantum state). In contrast to the flux result, it is possible for lobe penetration to be maximal in the two-frequency case. Lastly we close with a brief discussion of the nature of chaos in these systems: the horseshoe map paradigm generalizes to a *traveling horseshoe map sequence.* We point out that Noid and Stine [9], and more recently Goggin and Milonni [13], have also studied the quasiperiodically forced Morse oscillator; their approach differs from ours in that it is primarily a numerical study of absorption and the dissociation *threshold* for points initialized on the level set of the unperturbed Hamiltonian that corresponds to the *ground state,* and does not address the global picture of phase-space structure and transport afforded by the global stable and unstable manifolds. There have also been experimental studies of quasiperiodic electromagnetic forcing, such as Moorman *et al.* [30] on ionization of highly excited hydrogen atoms under a bichromatic microwave field.

We should stress at the outset the intent of our paper, for the scope of recent investigations of dissociation problems is quite vast and not without controversy, covering classical and/or quantum-mechanical studies (with or without comparisons) of regimes ranging from low-intensity microwave ionization of highly excited states to high-intensity infrared dissociation of ground states, along with chemical kinetics problems that cover a range of situations. Our interest here is in a classical study alone (i.e., the study of ensembles of classical phase-space trajectories), the reasoning being that before performing the difficult and somewhat controversial task of comparing classical and quantum-mechanical treatments of a classically chaotic system, it would be helpful to have a firm grounding in the classical extension from maps to sequences of maps.

II. THE QUASIPERIODICALLY FORCED MORSE OSCILLATOR AND ITS PHASE-SPACE STRUCTURE

We consider a quasiperiodically forced Morse oscillator

$$\begin{aligned} \dot{x} &= \frac{p}{m} , \\ \dot{p} &= -2D_0 a\,(e^{-ax} - e^{-2ax}) \\ &\quad + \epsilon d\,[E_1 \cos(\omega_1 t + \theta_{1_0}) + E_2 \cos(\omega_2 t + \theta_{2_0})] , \end{aligned} \tag{2.1}$$

$(x,p) \in \mathbb{R}^2$. One can think of $x \equiv r - r_e$ as the separation r of a two-atom molecule minus an equilibrium separation r_e, with p the relative momentum. The system then corresponds to a nonrotating pair of atoms interacting under a Morse potential and forced by an external two-frequency electromagnetic field with amplitudes ϵE_1 and ϵE_2. The parameters a and D_0 correspond to the range parameter and *unperturbed* dissociation energy, respectively, of the Morse potential, and d is the effective charge, or dipole gradient. The initial phases associated with the forcing are given by $\theta_{1_0}, \theta_{2_0}$. For concreteness, one can think of, say, a HF molecule, and hence set $m = 0.9571$ amu, $D_0 = 6.125$ eV, $a = 1.1741 r_B^{-1}$ (r_B is the Bohr radius), and $d = 0.7876 D_0 r_B^{-1}$. Note that, though for concreteness we consider dissociation of a diatomic molecule, a forced Morse oscillator can model other molecular phenomena, such as pumping a local mode of a polyatomic molecule by an infrared laser [10]. Further note that the rotating diatomic problem can be studied in the context of the k degree-of-freedom transport theory of Wiggins [31].

To study the dynamics of (2.1) it is advantageous to sample phase-space trajectories at discrete time intervals, the interval being one of the forcing periods, say $2\pi/\omega_2$.

For periodic forcing it is well understood that periodic sampling of trajectories leads to the study of a Poincaré map, which simplifies the underlying geometrical structure with which to study the motion; for quasiperiodic forcing, periodic sampling will in a similar way simplify the underlying structure to be studied. However, because of the lack of periodicity in the vector field time dependence, in this case we will be lead to the study of a bi-infinite sequence of maps. The evolution of system (2.1) from time $t=(2\pi/\omega_2)n$ to time $t=(2\pi/\omega_2)(n+1)$ defines a map on the plane

$$T_\epsilon(\cdot;n)\colon \mathbb{R}^2\to\mathbb{R}^2 ,$$

$$\left[x\left[\frac{2\pi}{\omega_2}n\right],p\left[\frac{2\pi}{\omega_2}n\right]\right] \to \left[x\left[\frac{2\pi}{\omega_2}(n+1)\right],p\left[\frac{2\pi}{\omega_2}(n+1)\right]\right] . \tag{2.2}$$

The goal then is to study the dynamics under the bi-infinite sequence of maps $\{T_\epsilon(\cdot;n);n\in Z\}$. To do this, we rewrite the Morse oscillator in autonomous form in order to construct invariant manifolds that are fixed in the resulting enlarged phase space. These manifolds form barriers which constrain the motion in the autonomous system phase space and hence form *structure* that governs motion in phase space. Having obtained these manifolds, we will use them to define for each time $t=(2\pi/\omega_2)n$ a set of curves in (x,p) space that will be used later to study the dynamics under the sequence of maps; in particular, to define the sequence of partial barriers between bounded and unbounded motion and the sequence of turnstiles.

The Morse oscillator in autonomous form is given by

$$\begin{aligned}\dot{x}&=\frac{p}{m} ,\\ \dot{p}&=-2D_0a(e^{-ax}-e^{-2ax})+\epsilon d(E_1\cos\theta_1+E_2\cos\theta_2) ,\\ \dot{\theta}_1&=\omega_1 ,\\ \dot{\theta}_2&=\omega_2 ,\end{aligned} \tag{2.3}$$

where $(\theta_1,\theta_2)\in T^2$, the 2-torus. We then define a Poincaré section

$$\Sigma^{\theta_{2_0}}=\{(x,p,\theta_1,\theta_2)|\theta_2=\theta_{2_0}\} ,$$

and the associated Poincaré map generated by the flow of (2.3) is given by

$$P_\epsilon\colon \Sigma^{\theta_{2_0}}\to\Sigma^{\theta_{2_0}} ,$$

$$(x(0),p(0),\theta_{1_0})\to\left[x\left[\frac{2\pi}{\omega_2}\right],p\left[\frac{2\pi}{\omega_2}\right],\theta_{1_0}+2\pi\frac{\omega_1}{\omega_2}\right] . \tag{2.4}$$

Studying the flow of (2.3) via this three-dimensional Poincaré map is equivalent to sampling the trajectories of (2.3) at time intervals equal to $2\pi/\omega_2$.

The phase portrait of the unperturbed Poincaré map $\bar{P}_{\epsilon=0}$ is portrayed in Fig. 1. There is a neutrally stable 1-torus at $\{(x,p,\theta_1)|x=p=0\}$ and a nonhyperbolic invariant 1-torus (of saddle-type stability) of the form

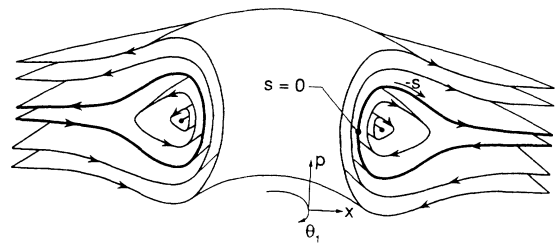

FIG. 1. Invariant manifolds of the unperturbed Poincaré map $P_{\epsilon=0}$, shown with a cutaway half-view. The separatrix is shown in boldface and is parametrized by (s,θ_1), where s is the time it takes for the point on the separatrix with (x,p) component $(x(-s),p(-s))$ to move to the point with (x,p) component $(x(0),p(0))$ (negative time intervals are included in this definition).

$$\tau_{\epsilon=0}=\{(x,p,\theta_1)|\lim x\to\infty,p=0\} . \tag{2.5}$$

The global stable and unstable manifolds of $\tau_{\epsilon=0}$, denoted $W^s(\tau_{\epsilon=0})$ and $W^u(\tau_{\epsilon=0})$, respectively, coincide to form a two-dimensional separatrix which *separates bounded and unbounded motion,* and which asymptotes with increasing x to $p=0$ (see the Appendix for the analytical expression of the separatrix). Any point initialized inside the separatrix evolves on a 2-torus and corresponds to a molecule which does not dissociate. Any point initialized outside the separatrix evolves on an unbounded two-dimensional surface, and corresponds to a molecule that is dissociated, asymptoting to infinite separation. As shown in Fig. 1, the separatrix is parametrized by (s,θ_1), where s is a timelike coordinate, described in the caption [$s=0$ is chosen to correspond to the point of symmetry $(x=-\ln(2)/a,p=0)$]. In Secs. IV and V we will be particularly interested in *phase slices* of the Poincaré section $\Sigma^{\theta_{2_0}}$, defined as $\chi(\bar{\theta}_1)\equiv\{(x,p,\theta_1)|\theta_1=\bar{\theta}_1\}$, and Fig. 2 shows the phase portrait in an arbitrary phase slice (for the unforced problem, the phase plane decouples from θ_1). The area enclosed by the separatrix in each phase

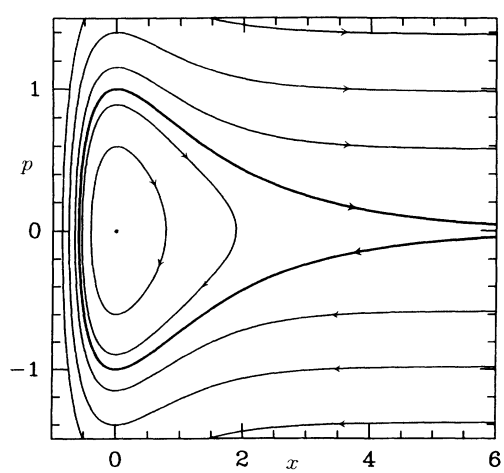

FIG. 2. The phase portrait in the two-dimensional phase slice $\chi(\bar{\theta}_1)$ of $\Sigma^{\theta_{2_0}}$. As shall be the case with all figures, x and p are plotted in units of Bohr radii and $\sqrt{2mD_0}$, respectively.

slice is equal to $4\pi D_0/\omega_0$, where $\omega_0 \equiv a(2D_0/m)^{1/2}$ is the frequency associated with simple harmonic motion near the bottom of the Morse well (this is in contrast to the study of MacKay and Meiss [7], who have an unbounded area enclosed by the separatrix for a Coulomb potential).

Quasiperiodic forcing causes the separatrix to undergo a *global bifurcation,* leading to nonintegrable motion near the unperturbed separatrix, and providing a mechanism for *escape* from bounded to unbounded motion, and *capture* from unbounded to bounded motion. The study of this bifurcation is complicated by the fact that the invariant saddle-type 1-torus is nonhyperbolic with infinite radius, and the relevant theorems, such as persistence of the invariant 1-torus, have been proven for normally hyperbolic tori with finite radii. For the Morse oscillator (2.3) we prove that the invariant 1-torus persists under forcing and obtain an expression for the 1-torus (see the Appendix). Given for the perturbed problem the existence of global differentiable stable and unstable manifolds of the surviving invariant 1-torus, the remaining theorems, such as those necessary for the generalized Melnikov construction, easily extend (see the Appendix). To avoid a lengthy digression to a rigorous mathematical discussion, we assume the existence of global differentiable stable and unstable manifolds, denoted $W^s(\tau_\epsilon)$ and $W^u(\tau_\epsilon)$, respectively, and present later some simple numerical computations that confirm the validity of the assumption. For $\epsilon > 0$, $W^s(\tau_\epsilon)$ and $W^u(\tau_\epsilon)$ are no longer identical, and Fig. 3 shows a case where the manifolds intersect in an infinity of 1-tori to produce the boundary of a complicated geometrical construct referred to as a *homoclinic tangle.* The manifolds crisscross each other *ad infinitum* to form the boundary of three-dimensional regions referred to as *lobes,* which shall be discussed more carefully as we go along. It is the homoclinic tangle and its lobes that form the phase-space structure needed to study molecular dissociation, and so as a first step we need to understand the geometry of this structure. For two-dimensional time-periodic systems (whose associated Poincaré map is two-dimensional), the geometrical possibilities are simple: the manifolds are one dimensional and either they never intersect, or they intersect in an infinity of points to form two-dimensional lobes. For more complicated time dependences and higher dimensions, the geometrical possibilities are far richer, but a generalized Melnikov theory provides an analytical tool for studying these geometries.

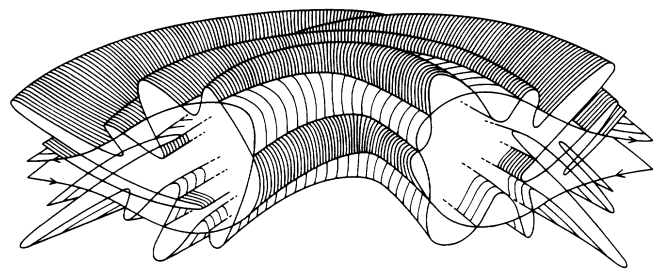

FIG. 3. A possible stable and unstable manifold geometry in $\Sigma^{\theta_{2_0}}$: the manifolds intersect in an infinity of 1-tori. There are other possible geometries, as discussed in Sec. III.

III. GENERALIZED MELNIKOV THEORY AND THE GEOMETRY OF THE HOMOCLINIC TANGLE

The generalized Melnikov function [32] is defined to be

$$M(s,\theta_1,\theta_2;\nu)=\int_{-\infty}^{\infty} DH(x_h(t),p_h(t))\cdot g(x_h(t),p_h(t),\omega_1 t+(\omega_1 s+\theta_1),\omega_2 t+(\omega_2 s+\theta_2);\mu)dt \ , \tag{3.1}$$

where

$$H(x,p)=\frac{p^2}{2m}+D_0(1-e^{-ax})^2$$

is the Hamiltonian of the unforced Morse oscillator, D denotes the derivative operator $(\partial/\partial x,\partial/\partial p)$ acting on $H(x,p)$,

$$\epsilon g(x,p,\theta_1,\theta_2;\mu)=(0,\epsilon d(E_1\cos\theta_1+E_2\cos\theta_2))$$

is the perturbation, (x_h,p_h) are the (x,p) coordinates of the unperturbed homoclinic separatrix, μ represents the perturbation parameters d, E_1, and E_2, and ν represents both the perturbation parameters and the other system parameters, m, D_0, and a. Expression (3.1) thus involves a timelike integral, along the *unperturbed* homoclinic separatrix, of a dot product between the perturbing vector field and the gradient of the *unperturbed* Hamiltonian (see Guckenheimer and Holmes [22] for an introduction to Melnikov theory and Wiggins [32] for an extensive study of generalized Melnikov theory). The main use of the Melnikov function is its provision of an $O(\epsilon)$ estimate of the separation $d(s,\theta_1,\theta_{2_0};\nu,\epsilon)$, normal to the unperturbed separatrix, of the perturbed stable and unstable manifolds in $\Sigma^{\theta_{2_0}}$ [32],

$$d(s,\theta_1,\theta_{2_0};\nu,\epsilon)=\frac{\epsilon M(s,\theta_1,\theta_{2_0};\nu)}{\|DH(x_h(-s),p_h(-s))\|}+O(\epsilon^2) \tag{3.2}$$

(see the Appendix and Fig. 4). This analytical estimate of

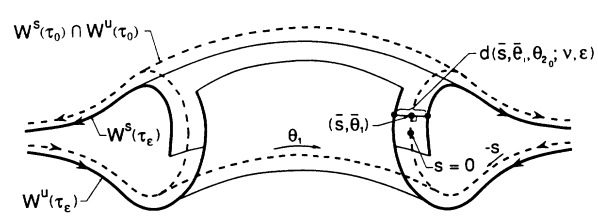

FIG. 4. The manifold separation $d(s,\theta_1,\theta_{2_0};\nu,\epsilon)$ normal to the unperturbed separatrix.

manifold separation is a powerful tool for studying many features of the homoclinic tangle, such as its geometry and, later on, the flux between bounded and unbounded motion. It is a straightforward consequence of the implicit function theorem [32] that within $O(\epsilon)$ of a zero of the Melnikov function (with $D_{(s,\theta_1)}M$ of rank one at the zero) is a transversal intersection of the stable and unstable manifolds, and we refer to this class of intersections as *primary intersection manifolds* (PIM's), which play a basic role in understanding tangle geometry. Hence the zero sets of the Melnikov function allow one to study the approximate location and the *exact* geometry of the PIM's.

For the quasiperiodically forced Morse oscillator (2.3) the Melnikov function is

$$M(s,\theta_1,\theta_2;\nu)=-\frac{2\pi}{a}[E_1 d e^{-\omega_1/\omega_0}\sin(\omega_1 s+\theta_1) + E_2 d e^{-\omega_2/\omega_0}\sin(\omega_2 s+\theta_2)] \quad (3.3)$$

(see the Appendix). Note that (3.3) is valid for $\omega_i \neq 0$, $i=1,2$; as explained in the Appendix, for either $\omega_1=0$ or $\omega_2=0$ (giving a constant term in the perturbation), the corresponding term in the Melnikov function vanishes. The Melnikov function is thus discontinuous at $\omega_i=0$, since the Melnikov amplitudes limit to a nonzero value as $\omega_i \to 0$, and we will discuss the physical implications of this discontinuity momentarily. Figure 5 shows comparisons between manifold separation computed by the Melnikov approximation (3.2) and by numerical computation of the manifolds using a *double-phase-slice* sampling method, which we describe later in the paper. The trigonometric dependence of the perturbation on $(t,\theta_{1_0},\theta_{2_0})$ in (2.1) carries through to a similar trigonometric dependence of M on (s,θ_1,θ_2) in (3.3) (the cosines go to sines). We refer to the absolute value of the ratio of the Melnikov amplitude in (3.3), $A_i \equiv -(2\pi/a)E_i d e^{-\omega_i/\omega_0}$, $i=1,2$, to the corresponding relative forcing amplitude $E_i d$ in (2.1) or (2.3) as a *relative scaling factor* $\mathcal{F}_{\mathrm{RSF}}$:

$$\mathcal{F}_{\mathrm{RSF}}(\omega_i;a,\omega_0) \equiv \left|\frac{A_i}{E_i d}\right| = \frac{2\pi}{a}e^{-\omega_i/\omega_0}. \quad (3.4)$$

The dependence of these factors on forcing frequency is described by a single *relative scaling function*

$$\mathcal{F}_{\mathrm{RSF}}(\omega;a,\omega_0)=\frac{2\pi}{a}e^{-\omega/\omega_0}. \quad (3.5)$$

The relative scaling function provides an approximate $[O(\epsilon)]$ measure of the effectiveness of a forcing frequency in producing manifold separation, and, as such, is a basic tool in understanding how each frequency affects dissociation. Since the function's exponential decay depends only on ω_0, the period associated with simple harmonic motion at the bottom of the Morse well provides the relevant time scale for the forcing's effectiveness at producing manifold separation. Given any two forcing frequencies, one immediately knows the relative importance of each one; for example, if one of the frequencies is at ω_0 and the other at $4\omega_0$, and the amplitudes of the two forcing terms are identical, then due to the exponential decay of the relative scaling function, the second term has a relatively negligible effect on manifold separation, and hence, as we shall later see, on certain transport properties, so that the problem is essentially one of single-frequency forcing. As another example, in the microwave limit $\omega_i \ll \omega_0$ the relative scaling factor associated with each frequency will be approximately $2\pi/a$, essentially frequency independent. We remark that, though the nonvanishing of the Melnikov amplitudes in the limit $\omega_i \to 0$ is not common (often they vanish in the limit of infinitely slow and infinitely fast forcing), this nonvanishing does occur in other systems, such as the forced Josephson junction [24,25].

In Fig. 6 we approximately portray [i.e., to $O(\epsilon)$] some PIM's in the Poincaré section $\Sigma^{\theta_{2_0}=0}$ by plotting the zero sets of $M(s,\theta_1,\theta_{2_0}=0;\nu)$ for a particular frequency ratio $\omega_2/\omega_1=g^{-1}$, where g is the golden mean $(\sqrt{5}-1)/2$, and a range of forcing amplitudes. Note that the Melnikov function, and hence the zero sets, are specified relative to the two-dimensional unperturbed separatrix, so that one interprets the plots in Fig. 6 in terms of the separatrix, shown by the dashed lines in Fig. 4, being flattened out onto a plane. Hence, though the PIM's live in the three-dimensional Poincaré section, they are close to the unperturbed separatrix and for ease of portrayal we suppress the dimension normal to the unperturbed separatrix.

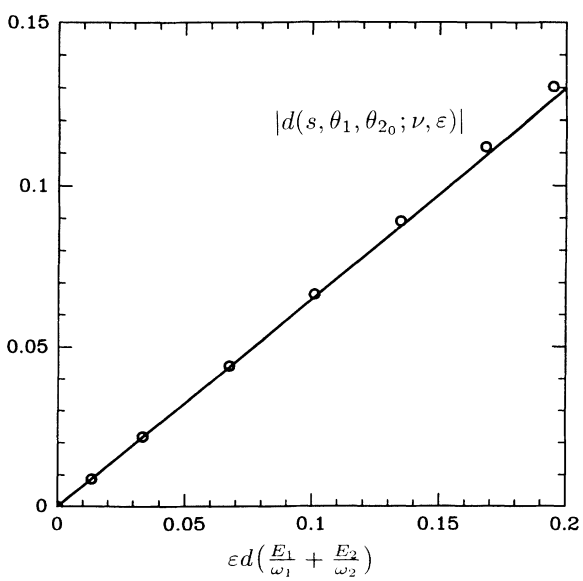

FIG. 5. A comparison between the manifold separation $|d(s,\theta_1,\theta_{2_0};\nu,\epsilon)|$ at $(s,\theta_1,\theta_{2_0})=(0,\frac{13}{8}\pi,\frac{3}{2}\pi)$, as computed by the Melnikov approximation (3.2) (the solid line) and by numerical simulation of the manifolds (open dots). For this example $(\omega_1,\omega_2)=2.6\omega_0(g,1)$, where g is the golden mean, $E_1 d=2.047\omega_0\sqrt{2mD_0}$, $E_2 d=3.685\omega_0\sqrt{2mD_0}$. The horizontal axis is the maximum value of the p coordinate of τ_ϵ [see Eq. (A4) in the Appendix] in units of $\sqrt{2mD_0}$.

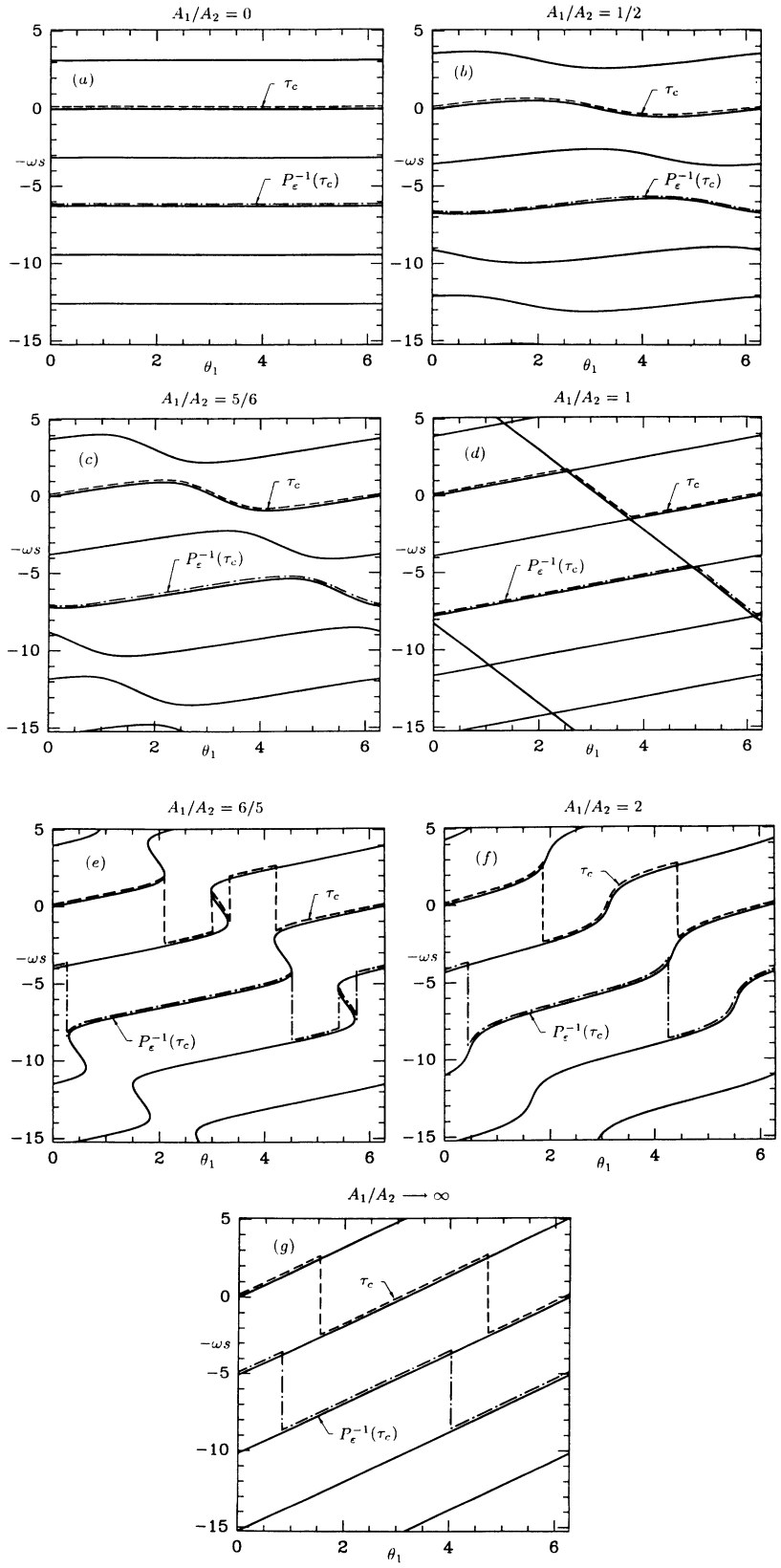

FIG. 6. Zero sets of the Melnikov function (3.3) for various ratios of Melnikov amplitudes A_1/A_2 and $\omega_1/g = \omega_2 \equiv \omega$. The dashed and dashed-dotted lines, τ_c and $P_\epsilon^{-1}(\tau_c)$, are defined and discussed in Sec. IV B. Note that these lines are really single-valued everywhere, and the vertical lines are merely for visual clarity.

Figures 6(a)–6(g) show PIM's for a range of ratios of Melnikov amplitudes. For $|A_1/A_2|<1$ the PIM's are nonintersecting 1-tori, for $|A_1/A_2|>1$ they are nonintersecting spirals, and for $|A_1/A_2|=1$ they are intersecting spirals (or equivalently intersecting 1-tori). For other ratios of ω_2/ω_1 (both commensurate and incommensurate), the PIM geometry, as A_1/A_2 is varied is qualitatively similar. In Beigie, Leonard, and Wiggins (henceforth BLW) [33,34] we provide a more detailed study of PIM geometry via theorems involving the Melnikov function. The basic result relevant to the Morse oscillator is the following. The manifolds $W^s(\tau_\epsilon)$ and $W^u(\tau_\epsilon)$ intersect if the Melnikov function (3.3) has a zero with $D_{(s,\theta_1)}M$ of rank one. One can easily see that the Melnikov function (3.3) passes through zero a countable infinity of times for each $\theta_1\in[0,2\pi)$. Thus, regardless of PIM geometry, the set of PIM's intersects each phase slice $\chi(\bar{\theta}_1)$ of the Poincaré section $\Sigma^{\theta_{2_0}}$ in a countable infinity of points for $\bar{\theta}_1\in[0,2\pi)$.

With an appreciation of PIM geometry, it should not be difficult to visualize the nature and geometry of the previously mentioned three-dimensional lobes in $\Sigma^{\theta_{2_0}}$ by remembering that the separation of $W^s(\tau_\epsilon)$ and $W^u(\tau_\epsilon)$, and hence the thickness of the lobes, is normal to the page for Fig. 6 (see Fig. 7). As one might expect from the figures, the geometries of the invariant lobes can take on a rich variety in quasiperiodic problems, and thus a precise definition of an invariant three-dimensional lobe in $\Sigma^{\theta_{2_0}}$ necessitates fairly careful development and a rather abstract description. We merely say here that for the case where PIM's are 1-tori, a *lobe* in $\Sigma^{\theta_{2_0}}$ is the region bounded by segments of $W^s(\tau_\epsilon)$ and $W^u(\tau_\epsilon)$ between adjacent PIM's; for other PIM geometries a definition similar in spirit applies and we refer the reader to BLW [33,34].

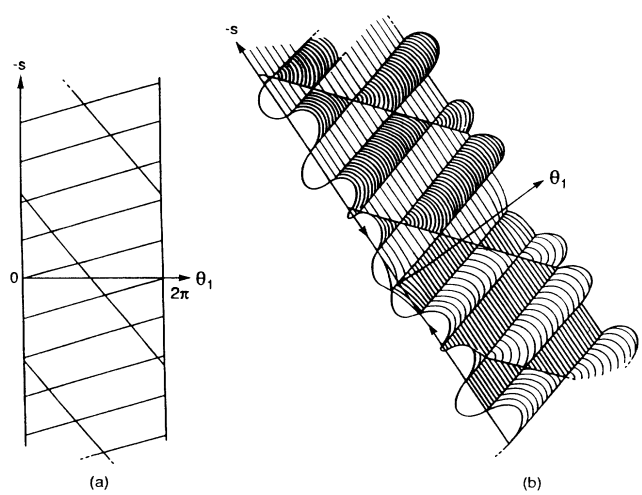

FIG. 7. Visualizing three-dimensional lobes by showing the suppressed dimension.

IV. THE HOMOCLINIC TANGLE AS A TEMPLATE FOR STUDYING MOLECULAR DISSOCIATION

A. Using the invariant homoclinic tangle to study the sequence of maps

We have a set of two-dimensional invariant manifolds $W^s(\tau_\epsilon)$ and $W^u(\tau_\epsilon)$ fixed in the three-dimensional Poincaré section $\Sigma^{\theta_{2_0}}$ for the Morse oscillator in autonomous form (2.3), and the geometry of the manifolds is studied via the generalized Melnikov function. The trick is then to relate things back to the original physical problem, that of a sequence of two-dimensional maps on (x,p) space. This is done in a simple manner, as described heuristically here and rigorously in BLW [33,34]. At each sample time $t=(2\pi/\omega_2)n$, the phase associated with the first forcing frequency is $\theta_1(n)=\theta_{1_0}+2\pi(\omega_1/\omega_2)n$; hence one can think of the original two-dimensional Morse oscillator (2.1) at this sample time as a *two-dimensional slice* of the three-dimensional Poincaré section $\Sigma^{\theta_{2_0}}$, defined by the *time slice,* or equivalently the *phase slice*

$$\chi\left[\theta_{1_0}+2\pi\frac{\omega_1}{\omega_2}n\right]=\left\{(x,p,\theta_1)\,\middle|\,\theta_1=\theta_{1_0}+2\pi\frac{\omega_1}{\omega_2}n\right\}. \tag{4.1}$$

Hence the sequence of maps (2.2) on (x,p) space can be understood in terms of P_ϵ acting on a sequence of phase slices of $\Sigma^{\theta_{2_0}}$, as shown in Fig. 8 (for incommensurate frequencies the phase slices will visit $\theta_1\in[0,2\pi)$ uniformly and densely, and for commensurate frequencies they will visit a finite number of θ_1 values). The intersection of each time slice with $W^s(\tau_\epsilon)$ and $W^u(\tau_\epsilon)$ defines *time-dependent* one-dimensional manifolds in (x,p) space at the appropriate sample time [the manifolds vary with the time slice since $W^s(\tau_\epsilon)$ and $W^u(\tau_\epsilon)$ vary with θ_1]. Figure 8 illustrates this in the case where the invariant manifolds intersect in 1-tori, and the result for each time slice is a time-dependent two-dimensional homoclinic tangle with the same topological constraints as in the familiar case of periodic forcing: the two manifolds crisscross *ad infinitum,* intersecting each other but never intersecting themselves, to define a countable infinity of two-dimensional *lobes.* More precisely, the set of PIM's intersect the time slice $\chi(\theta_{1_0}+2\pi(\omega_1/\omega_2)n)$ in a countable infinity of *primary intersection points* (PIP's), and the segments of $W^s(\tau_\epsilon)$ and $W^u(\tau_\epsilon)$ in that time slice between adjacent PIP's define the boundary of a two-dimensional lobe in that slice. The template for transport in (x,p) space under the sequence of maps, and hence the key to studying molecular dissociation, is thus the time-dependent two-dimensional lobe structure associated with each sample time. It is a straightforward consequence of the invariance of $W^s(\tau_\epsilon)$ and $W^u(\tau_\epsilon)$ that each lobe in the nth time slice maps under $T_\epsilon(\cdot;n)$ to a lobe in the $(n+1)$th time slice. Hence the global picture for transport in (x,p) space under the sequence of maps $\{T_\epsilon(\cdot;n)|n\in Z\}$ is expressed in terms of lobes mapping

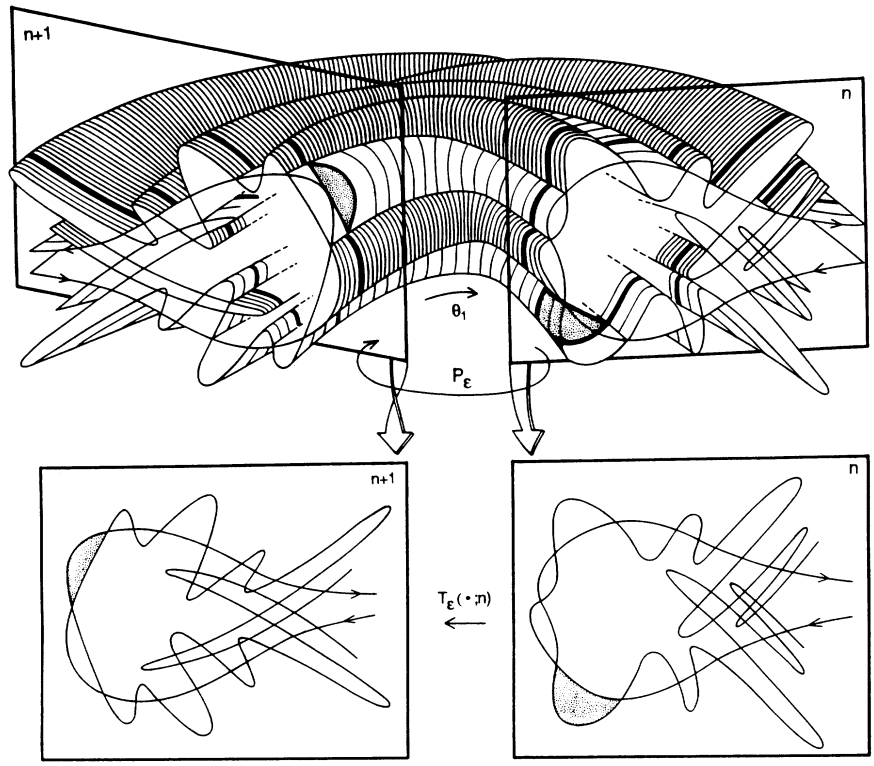

FIG. 8. Two successive time slices of the invariant three-dimensional lobe structure in $\Sigma^{\theta_{2_0}}$ define two successive time-dependent two-dimensional lobe structures in (x,p) space.

within a sequence of two-dimensional lobe structures derived from invariant manifolds embedded in a three-dimensional Poincaré section (as shown in Fig. 9). We should stress that, as a consequence of invariance, for any invariant manifold geometry there is a two-dimensional lobe structure for *each* time slice in any particular sequence of time slices.

To describe transport in phase space necessitates specifying how the two-dimensional lobes map from one to another under the sequence of maps. At first this may seem a daunting task, since one needs to address a bi-infinite sequence of maps. However, this task is greatly simplified by the fact that the $(\dot{x},\dot{p})$ equations in (2.3) depend periodically on θ_1 for fixed (x,p,θ_2), so we only need consider the finite interval $\theta_1 \in [0,2\pi)$; hence one can describe any map in the sequence of maps in terms of P_ϵ acting on $\chi(\bar{\theta}_1)$ for some $\bar{\theta}_1 \in [0,2\pi)$. The invariant manifolds are central to such a description, for once one

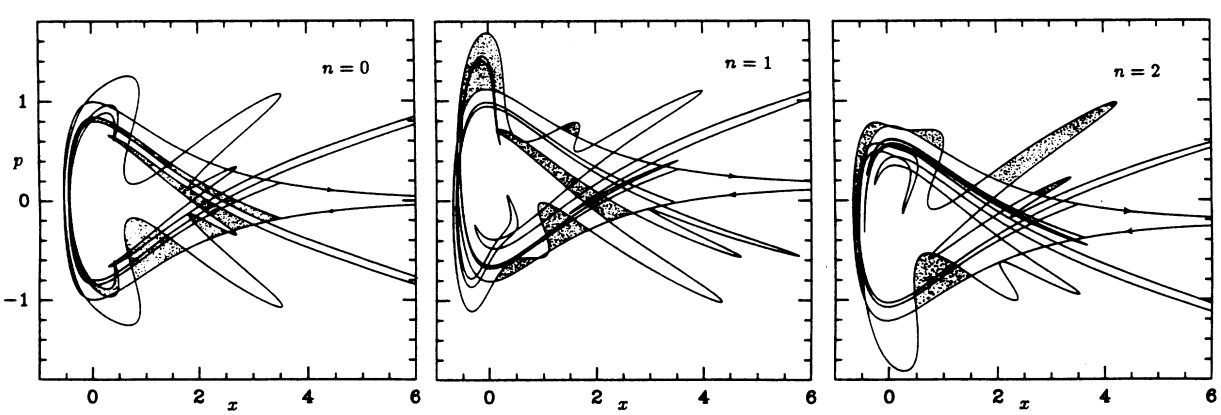

FIG. 9. Two-dimensional lobes mapping within the sequence of lobe structures (the shaded lobes map in an orientation- and order-preserving manner). Numerical computation of the lobe structures is discussed in Sec. V A. For this example $(\omega_1,\omega_2)=(1,g)2.665\omega_0$, $\epsilon d(E_1,E_2)=(0.590,0.213)\omega_0\sqrt{2mD_0}$, and $(\theta_{1_0},\theta_{2_0})=(\pi,0)$. Since we will return to this case, note that the perturbation amplitudes are chosen to give equal Melnikov amplitudes, so that the problem is similar to the one in Fig. 6(d), except that here we sample at the slower frequency.

knows how the three-dimensional lobes in $\Sigma^{\theta_{2_0}}$ evolve under the *single* map P_ϵ, one can easily deduce how the two-dimensional lobes evolve under any of the maps in the sequence of maps (several examples and illustrations are given in BLW [33,34]). Recognizing the importance of the invariant manifolds, we proceed to discuss the aspects of transport that are relevant to the study of molecular dissociation. The key issue is to use the sequence of lobe structures to *precisely* define boundaries between bounded and unbounded motion and then *precisely* identify the regions in phase space which cross these boundaries under each map.

B. Deriving from the homoclinic tangle the sequence of partial barriers between regions of bounded and unbounded motion and the sequence of turnstiles

By definition, points on $W^s(\tau_\epsilon)$ and $W^u(\tau_\epsilon)$ asymptote with positive and negative time, respectively, to the invariant 1-torus at infinity τ_ϵ, so that in a manner similar to the separatrix of the unforced system, $W^s(\tau_\epsilon)$ and $W^u(\tau_\epsilon)$ play the role of dividing surfaces between bounded and unbounded motion. For the unforced problem, where $W^s(\tau_{\epsilon=0})$ and $W^u(\tau_{\epsilon=0})$ are identical, the *entire* manifolds play the role of the dividing surface and they act as a *complete barrier.* For the forced problem, where $W^s(\tau_\epsilon)$ and $W^u(\tau_\epsilon)$ are no longer identical, *segments* of the manifolds, joined together at an intersection set, play the role of the dividing surface between bounded and unbounded motion; it is possible for points to move across this surface, and hence the dividing surface acts as a *partial barrier.* We give a careful discussion of the construction of these dividing surfaces in BLW [33,34], and the essentials of this construction applied to the Morse oscillator can be conveyed here in a simple manner with the help of some figures. One chooses the above-mentioned intersection set to be a one-dimensional subset of the set of PIM's that is piecewise continuous and intersects each phase slice $\chi(\bar{\theta}_1)$, $\bar{\theta}_1 \in [0,2\pi)$, in a single point. Examples are illustrated in Fig. 6, denoted by τ_c (there are, of course, other possible choices, and we will discuss our particular choice momentarily). If we let $S[\tau_\epsilon,\tau_c]$ and $U[\tau_\epsilon,\tau_c]$ denote the segments of $W^s(\tau_\epsilon)$ and $W^u(\tau_\epsilon)$, respectively, from τ_ϵ to τ_c, then $\mathcal{C} \equiv U[\tau_\epsilon,\tau_c] \cup S[\tau_\epsilon,\tau_c]$ denotes a two-dimensional surface in $\Sigma^{\theta_{2_0}}$ that divides *each phase slice* $\chi(\bar{\theta}_1)$, $\bar{\theta}_1 \in [0,2\pi)$, into two regions, as illustrated in Fig. 10. For the case of toral PIM's, illustrated in Fig. 10(a), one can choose τ_c to be a 1-torus, and $\mathcal{C}$ in fact divides $\Sigma^{\theta_{2_0}}$ into two regions; for the case of spiral PIM's, illustrated in Fig. 10(b), one must choose τ_c to have a discontinuity, and hence $\mathcal{C}$ is discontinuous and does *not* divide $\Sigma^{\theta_{2_0}}$ into two regions, since there are gaps at the region of discontinuity. However, for all cases, $\mathcal{C}$ divides each *phase slice* $\chi(\bar{\theta}_1)$, $\bar{\theta}_1 \in [0,2\pi)$, into two regions, which is all one is interested in for the sequence of maps. At each sample time $t=(2\pi/\omega_2)n$, we thus have in (x,p) space a time-dependent boundary $\mathcal{C}(n) \equiv \mathcal{C} \cap \chi(\theta_{1_0} + 2\pi(\omega_1/\omega_2)n)$ that divides the space into two regions, denoted $R_b(n)$ and $R_u(n)$, as illustrated in Fig. 10 (note that invariant three-dimensional regions in $\Sigma^{\theta_{2_0}}$, R_u and R_b, are then defined as the union of the corresponding two-dimensional regions over the phase slices defined by $\bar{\theta}_1 \in [0,2\pi)$). In the context of this time-dependent boundary we can now explain the choice of τ_c in Fig. 6, and hence the choice of the sequence of boundaries. We chose τ_c such that for each $\bar{\theta}_1 \in [0,2\pi)$ the s parameter associated with $\tau_c \cap \chi(\bar{\theta}_1)$ is the closest to zero out of all the PIM intersections with that phase

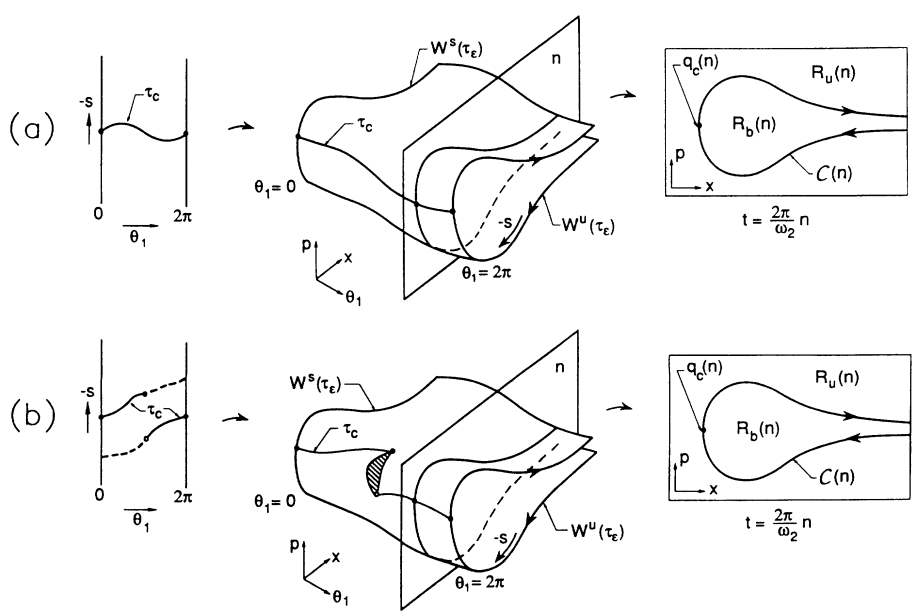

FIG. 10. The invariant boundary $\mathcal{C}$ divides each phase slice into two regions: an illustration for (a) toral PIM geometry and (b) spiral PIM geometry $[q_c(n) \equiv \tau_c \cap \chi(\theta_{1_0} + 2\pi(\omega_1/\omega_2)n)]$. The shaded region shows a gap.

slice. The aim of this choice is for the boundary $\mathcal{C}(n)$ to most closely resemble the unperturbed separatrix at each time slice.

As we shall explain, points can cross $\mathcal{C}$ *only* via the *turnstile lobes,* which we now define and identify. It is a straightforward consequence of the orientation preserving nature of P_ϵ that the lobes between τ_c and $P_\epsilon^{-1}(\tau_c)$, which we refer to as the *turnstiles,* change their orientation *relative to* $\mathcal{C}$ under P_ϵ. What we mean by this can be easily visualized in Fig. 11, where we show an example with toral PIM's and one pair of turnstile lobes. It should be clear from the figure that points in the turnstiles, and *only* these points, cross the invariant boundary $\mathcal{C}$ under P_ϵ, mapping from outside to inside or vice versa. At each sample time $t=(2\pi/\omega_2)n$, we thus have in (x,p) space time-dependent turnstiles defined by

$$L_{bu}(1;n)\equiv L_{bu}(1)\cap\chi\left[\theta_{1_0}+2\pi\frac{\omega_1}{\omega_2}n\right],$$
$$L_{ub}(1;n)\equiv L_{ub}(1)\cap\chi\left[\theta_{1_0}+2\pi\frac{\omega_1}{\omega_2}n\right], \tag{4.2}$$

where $L_{bu}(1)$ and $L_{ub}(1)$ are the three-dimensional lobes in $\Sigma^{\theta_{2_0}}$ that map under one iterate of P_ϵ from R_b to R_u and from R_u to R_b, respectively. Hence the turnstile $L_{bu}(1;n)$ $[L_{ub}(1;n)]$ is the set of lobes which map under $T_\epsilon(\cdot;n)$ from *inside (outside)* $R_b(n)$ to *outside (inside)* $R_b(n+1)$, and we shall refer to these two processes as *escape* and *capture,* respectively. The points in $R_b(n)$ at time $t=(2\pi/\omega_2)n$ are destined to oscillate in a bounded fashion until at some future sample time $t=(2\pi/\omega_2)\tilde{n}$, $\tilde{n}>n$ (which may or may not ever occur), they *escape* under $T_\epsilon(\cdot;\tilde{n})$ *via the turnstile lobes* $L_{bu}(1;\tilde{n})$ to $R_u(\tilde{n}+1)$ and henceforth asymptote to infinite separation (in a similar manner one describes capture). Hence, it is correct to interpret $R_b(n)$, $R_u(n)$ as the regions of bounded and unbounded motion, respectively, and the turnstile lobes $L_{bu}(1;n)$ and $L_{ub}(1;n)$ as the *sole* mechanism for transport between the bounded and unbounded regions.

We conclude this section with three remarks.

(i) Previous studies which do not address invariant manifolds are forced to use approximate and somewhat *ad hoc* criteria for dissociation. For example, in their study of ionization and dissociation in terms of a forced nonlinear oscillator, Leopold and Percival [1] (Coulomb potential, periodic forcing), and later Goggin and Milonni [12,13] (Morse potential, periodic and quasiperiodic forcing) use for their dissociation criterion a time-dependent "compensated energy": any point with energy greater than this compensated energy is considered dissociated. As we shall see with some simulations in Sec. V A, it is possible for their criterion to significantly differ from the true criterion offered by the invariant manifolds. Even if one is in a regime where such an approximation works well, it is still important to appreciate the true dissociation criterion.

(ii) We stress the new feature in the generalization from transport under *maps* to transport under *sequences of maps:* one is not concerned with transport with respect to a fixed region in the plane, as is the case with two-dimensional maps, but with transport with respect to a sequence of regions, which vary in shape and size from one time sample to the next. This is a consequence of the fact that the relevant dividing lines between bounded and unbounded motion, made up of points which asymptote to the invariant torus τ_ϵ as $x\to\infty$, vary from one time sample to the next, due to the more complicated time dependence in the forcing. That the time-dependent tem-

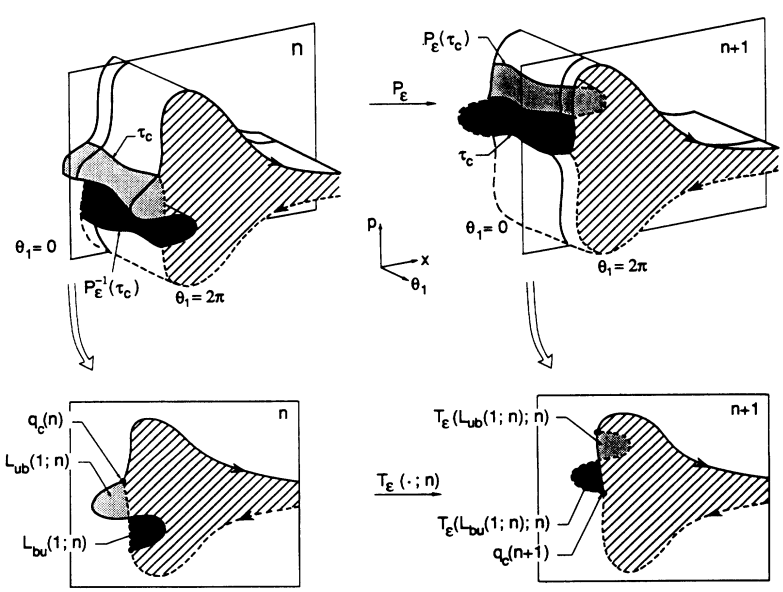

FIG. 11. The turnstiles as the sole mechanism for transport between the bounded and unbounded regions.

plate with which to study transport, the sequence of lobe structures, is derived from a set of invariant manifolds embedded in an enlarged phase space, allows one to embrace the more complicated transport issues associated with quasiperiodic forcing.

(iii) Though not explicitly stated, our discussion of turnstile lobes assumed that each lobe was entirely contained in one region or the other. This is the case for small enough forcing (which in practice can be quite large), and when it is not the case one can redefine the turnstiles in an appropriate manner to be the portions in one of the regions [33–35].

C. A comment on boundedness and unboundedness in the quantum-mechanical treatment

For a classical approach, it is the segments of the invariant manifolds of the *perturbed* system, and *not* the unperturbed separatrix, that are relevant to the criterion for dissociation. For example, in the forced system a point may oscillate in a bounded manner over some finite time interval such that it repeatedly crosses back and forth over the unperturbed separatrix. Bearing this in mind, consider the conventional approach used in the quantum-mechanical treatment (as described, for example, in Goggin and Milonni [12,13] and Lu *et al.* [14], or elementary quantum-mechanics texts for that matter). Let $\{|b_i\rangle\}$ denote the set of bound states of the *unforced* Morse oscillator. If the system is initially in some bound state $|\psi(t=0)\rangle$ then the dissociation probability at time t for the forced problem is

$$P_d(t)=1-\sum_i |\langle b_i|\psi(t)\rangle|^2 . \tag{4.3}$$

Hence one finds the dissociation probability by subtracting from one the probability of being in one of the $\{|b_i\rangle\}$ states. The obvious question that arises for this approach is: does one want to interpret $\{|b_i\rangle\}$ as the set of bound states for the *forced* problem? For time-independent perturbations (Zeeman effect, Stark effect, and so forth) one routinely solves for the perturbed eigenvalues and eigenstates; however, for the more difficult case of time-dependent perturbations it has become common to study transitions relative to the *unperturbed* basis states according to (4.3) and the question of the interpretation of bounded and unbounded motion in the time-dependent problem remains largely ignored.

V. QUANTIFYING FLUX AND DISSOCIATION RATES

A. Computing the partial barriers between bounded and unbounded motion, the number of turnstile lobes, and the turnstile boundaries

A first step towards quantifying molecular dissociation via phase-space transport is the numerical computation of the partial barriers and turnstiles, which provides a direct portrayal of phase-space structure and allows exact computation of flux and various dissociation rates. The procedure for numerical computation of the invariant stable and unstable manifolds of saddle-type fixed points of maps at finite (x,p) values is well known and straightforward; the added complications here are of course that we are dealing with sequences of maps and an invariant 1-torus with infinite radius. One can study sequences of maps by employing a *double-phase-slice sampling method* [33,34], which is similar to the sampling method for maps, except that one takes into account that the evolution from one time sample to the next is understood in terms of phase slices of the Poincaré section $\Sigma^{\theta_{2_0}}$ mapping from one to another under P_ϵ. Hence to compute segments of the global stable and unstable manifolds in some finite window $x\in[x_a,x_b]$ at a given time sample $t=(2\pi/\omega_2)n$, i.e., at a given phase slice $\chi(\theta_{1_0}+2\pi(\omega_1/\omega_2)n)$, one evolves under the dynamical system vector field backward and forward in time, respectively, over some time interval $|\Delta t|=(2\pi/\omega_2)j$, $j\in Z$, small segments of the stable and unstable manifolds that originate at large x values in the *different* phase slices $\chi(\theta_{1_0}+2\pi(\omega_1/\omega_2)(n+j))$ and $\chi(\theta_{1_0}+2\pi(\omega_1/\omega_2)(n-j))$, respectively. If τ_ϵ had a finite radius, one would take these initial segments to be the local stable and unstable manifolds of τ_ϵ in the appropriate phase slices. The p coordinate of τ_ϵ is known exactly in any phase slice [see Eq. (A4) in the Appendix], so in practice one can take the initial segments to be horizontal segments at large x values (say $x>20$) slightly above and below the p value of $\tau_\epsilon\cap\chi(\theta_{1_0}+2\pi(\omega_1/\omega_2)(n+j))$ and $\tau_\epsilon\cap\chi(\theta_{1_0}+2\pi(\omega_1/\omega_2)(n-j))$ for $W^s(\tau_\epsilon)$ and $W^u(\tau_\epsilon)$, respectively. The error incurred by this approximation can be made negligible by choosing for the line segment x sufficiently large and p sufficiently close to the p coordinate of τ_ϵ in the appropriate phase slice (for example, in the Melnikov calculations in Fig. 5 we ensure that the error due to the initial segment approximation is orders of magnitude smaller than the true manifold separation). In making this approximation, we stress the need to respect the variation of the p coordinate of τ_ϵ with the choice of Poincaré section and phase slice: in the context of periodic forcing, Bruhn [36] takes the initial segment to lie on the corresponding *unperturbed* manifolds, but for reasonably sized perturbations a line element that lies on $W^s(\tau_{\epsilon=0})$ can lie *below* $W^u(\tau_\epsilon)$, and hence move *opposite* to the intended direction.

With the above procedure one can calculate with arbitrary precision segments of the invariant manifolds for the nth time sample, and from this immediately calculate the partial barriers and turnstile boundaries by an appropriate choice of $\tau_c\cap\chi(\theta_{1_0}+2\pi(\omega_1/\omega_2)n)$ and $\tau_c\cap\chi(\theta_{1_0}+2\pi(\omega_1/\omega_2)(n+1))$, and then the calculation of $P_\epsilon^{-1}(\tau_c\cap\chi(\theta_{1_0}+2\pi(\omega_1/\omega_2)(n+1)))$. Figure 12 shows a simple illustration with a sequence of four time slices. Note how the number, size, and shape of the turnstile lobes can change from one time sample to the next, which contrasts sharply with the time-periodic case, where the turnstiles are independent of sample time. By explicit computation of the manifolds as just described here, one can determine the number of turnstile lobes for each time slice. However, the Melnikov function provides an analytical tool for determining turnstile lobe number, which will be relevant to some of the flux calcu-

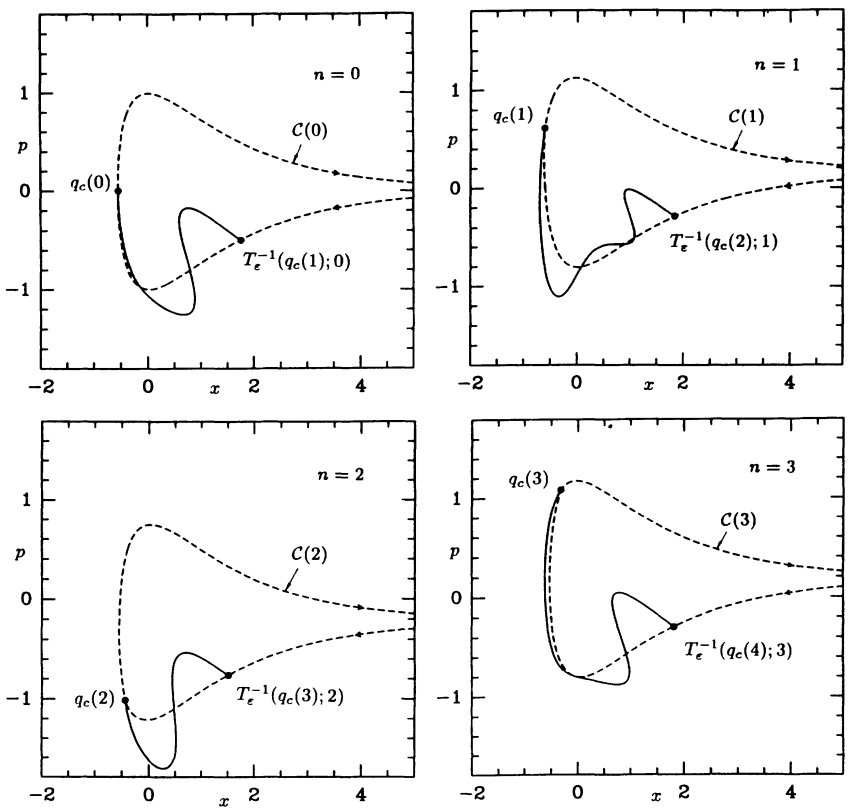

FIG. 12. The turnstiles and core boundaries for a sequence of four time slices $[q_c(n) \equiv \tau_c \cap \chi(\theta_{1_0}+2\pi(\omega_1/\omega_2)n)$ and the parameters are the same as in Fig. 9].

lations to come. If $s = s_c(\theta_1)$ denotes the s values associated with the choice of τ_c, then the turnstile lobes at the nth time slice lie between $s_c(\theta_{1_0}+2\pi(\omega_1/\omega_2)n)$ and $s_c(\theta_{1_0}+2\pi(\omega_1/\omega_2)(n+1))+2\pi/\omega_2$. Every time the Melnikov function crosses through zero it corresponds to a nearby crossing of the stable and unstable manifolds; hence, if $\mathcal{N}(\theta_{1_0}+2\pi(\omega_1/\omega_2)n)$ denotes the number of zero crossings of $M(s,\theta_{1_0}+2\pi(\omega_1/\omega_2)n,\theta_{2_0};\nu)$ between (and not counting) the above two endpoints, then the number of turnstile lobes in that time sample is (generically) given by $\mathcal{N}(\theta_{1_0}+2\pi(\omega_1/\omega_2)n)+1$ (and by the sign of the Melnikov function one can determine how many of these lobes correspond to escape and how many to capture, as described in BLW [33,34]. Bearing this in mind, the plots of the Melnikov zero sets in Fig. 6, along with the portrayal of τ_c and $P_\epsilon^{-1}(\tau_c)$, allow one to immediately deduce the number of turnstile lobes in each phase slice. For example, in Fig. 6(d) there is seen to be two turnstile lobes (one capture and one escape) for all time slices (except the isolated cases where the PIM's cross). In contrast, in Fig. 12, which is the same example except sampled now at the slower rather than the faster frequency, there is a different number of turnstiles lobes (ranging from two to four) for each time slice. BLW [33,34] give a careful comparison of the effect of different sampling choices; for either choice, however, the same transport formalism goes through and we will on purpose consider both types of sampling interchangeably.

In Fig. 13 we compare for a particular example the dissociation criterion based on numerical computation of segments of the invariant manifolds versus Leopold and Percival's "compensated energy." The compensated energy includes a time-dependent term that simply shifts the unperturbed separatrix up and down in p with time, and there is no accounting for the overall distortion and "breathing" of the true partial barriers.

B. Turnstile lobe area and flux

A central transport quantity in previous studies of molecular dissociation in the context of maps is the *flux* between regions of bounded and unbounded motion [7,15–21,37–39]. Though flux describes an important feature of transport to and from regions of bounded and unbounded motion, we shall later see its limitations. In contrast to the case of area-preserving maps, where a single measure of flux suffices, for area-preserving sequences of maps there are five relevant measures of flux. The first two are the *instantaneous flux,* denoted $\phi_e(n)$ and $\phi_c(n)$ for escape and capture, respectively,

$$\phi_e(n)=\frac{\omega_2}{2\pi}\mu(L_{bu}(1;n)) ,$$
$$\phi_c(n)=\frac{\omega_2}{2\pi}\mu(L_{ub}(1;n)) , \tag{5.1}$$

where $\mu(\ )$ denotes the area of the lobes within the parentheses. Instantaneous flux thus refers to the area in phase space, per sample time, that escapes or is captured between the nth and $(n+1)$th time samples, and is in general different for each time sample and for escape versus capture, since the partial barriers vary with each time slice and the area of the region they enclose can change. The next two are the *finite-time average flux,* denoted $\Phi_e(n)$ and $\Phi_c(n)$ for escape and capture, respectively, which are simply the average of the instantaneous flux over the first $n+1$ time samples. This as well is different for each n and for escape versus capture, and though both quantities will converge to the same value in the limit $n\to\infty$, the convergence time can vary from being quite short to quite long. The final measure is the *infinite-time average flux*

$$\Phi=\lim_{N\to\infty}\frac{1}{2(N+1)}\sum_{n=0}^{N}[\phi_e(n)+\phi_c(n)] , \tag{5.2}$$

which is the same for escape and capture, since the area of $R_b(n)$ remains bounded, as should be plain from the definition of $R_b(n)$. One can exactly compute the above fluxes by identifying the turnstiles and computing their boundaries for each time slice, as described in Sec. V A.

One can approximately [to $O(\epsilon)$] compute the fluxes using the Melnikov function. Integrating the distance expression over the arc length of the unperturbed separatrix

$$d\lambda=\|DH(x_h(-s),p_h(-s))\|ds$$

gives the area of an individual turnstile lobe $\mathcal{L}(1;n)\subseteq L_{bu}(1;n)\cup L_{ub}(1;n)$ in the nth time slice $\chi(\theta_{1_0}+2\pi(\omega_1/\omega_2)n)$,

$$\mu(\mathcal{L}(1;n))=\epsilon\int_{s_a(n)}^{s_b(n)}\left|M\left[s,\theta_{1_0}+2\pi\frac{\omega_1}{\omega_2}n,\theta_{2_0};\nu\right]\right|ds + O(\epsilon^2) , \tag{5.3}$$

where $s_a(n)<s_b(n)$ are the s values of the bounding PIP's of the lobe. Using (5.3), one can calculate instantaneous flux and finite-time average flux by determining the areas of the appropriate turnstile lobes (see Figs. 14 and 15). For the infinite-time average, one obtains a particularly simple expression

$$\Phi=\lim_{T\to\infty}\frac{\epsilon}{2T}\int_0^T|M(s,\theta_{1_0},\theta_{2_0};\nu)|ds+O(\epsilon^2) . \tag{5.4}$$

The expression for Φ really involves a sum over phase slices of the turnstile lobe areas, for which the $O(\epsilon)$ term of (5.3) is a good approximation for ϵ not too large and ω_1,ω_2 not too small, but this is converted to an integral over a *single* phase slice by elementary periodicity properties of the Melnikov function arguments [33,34]. Note that, for a given sampling phase θ_{2_0}, for commensurate frequencies the average flux depends on the initial phase θ_{1_0}, i.e., $\Phi=\Phi(\theta_{1_0})$, but for incommensurate frequencies it is independent of θ_{1_0}.

One would like to compare the flux associated with periodic and quasiperiodic forcing. A normalization criterion for the forcing amplitudes is needed to decide upon "equivalent" periodic and quasiperiodic perturbations that can be compared. For example, let us choose the criterion $E_1^2+E_2^2=\text{const}\equiv E^2$ (i.e., as E_1 and E_2 are varied, we keep constant the sum of the intensities associated with each amplitude in the electromagnetic field). For fixed ω_1,ω_2, we then vary, say, E_1 from 0 to E, with E_2 determined by the normalization criterion. The question then is how does the infinite-time average flux vary as a function of E_1? The variation depends on two properties: interference effects and relative scaling factors. Referring to Fig. 16, at the single-frequency limits, associated with the endpoints $E_1=0$ and $E_1=E$, the average flux Φ is proportional to the relative scaling factor associated with the corresponding frequency. Interference

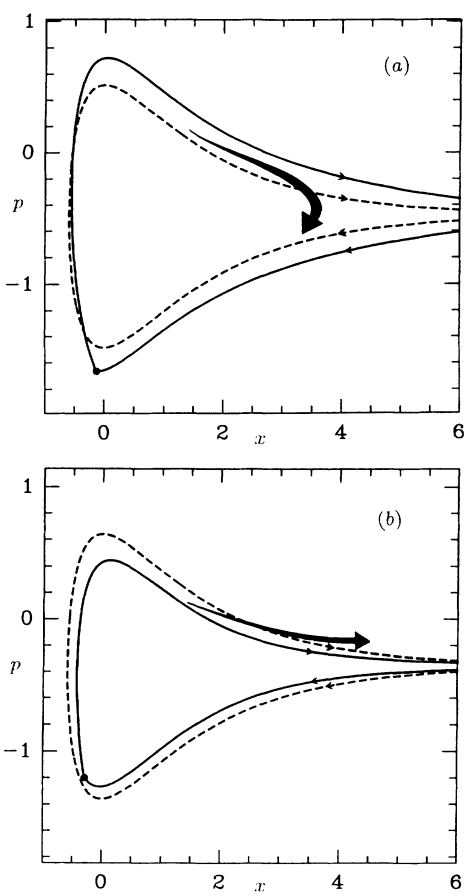

FIG. 13. The dissociation criterion based on segments of the stable and unstable manifolds (the solid line) and Leopold and Percival's compensated energy (the dashed line). For this example we are in the phase slice $\chi(\theta_1=\frac{23}{22}\pi)$ of the Poincaré section $\Sigma^{\theta_{2_0}=3\pi/2}$, and the parameters are (a) $(\omega_1,\omega_2)=\omega_0(0.231,2.618)$, $\epsilon d(E_1,E_2)=(0.102,1.105)\omega_0\sqrt{2mD_0}$; (b) the same as (a) except $E_1\to -E_1$. Note that for this particular example we choose $q_c(n)$ whose s value is *second* closest to zero, which leads to a smoother core boundary in this case.

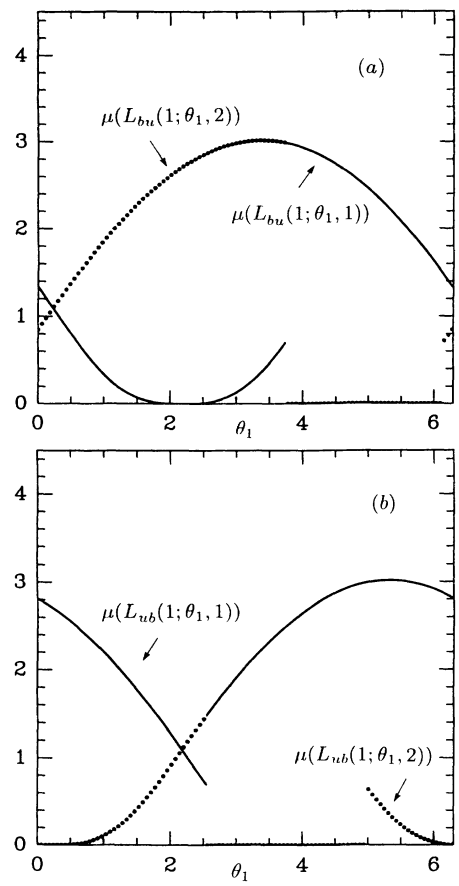

FIG. 14. The variation of turnstile lobe area with the phase θ_1. In this example there are one or two of each of the escape and capture turnstile lobes, depending on the phase slice: $L_{bu}(1;\theta_1,j)$ and $L_{ub}(1;\theta_1,j)$ denote the jth escape and capture turnstile lobes, respectively, in the phase slice defined by θ_1, where j increases with s. Note that different lobes correspond to different line types, which are discontinuous in θ_1. For this example we are in the Poincaré section $\Sigma^{\theta_{2_0}=0}$ with Melnikov amplitudes $(A_1,A_2)\equiv-(A,A)$, $A>0$, and $(\omega_1,\omega_2)=(g^{-1},1)\omega_0$. The areas for the escape and capture lobes are given in (a) and (b), respectively, and are per unit $\epsilon A/\omega_0$.

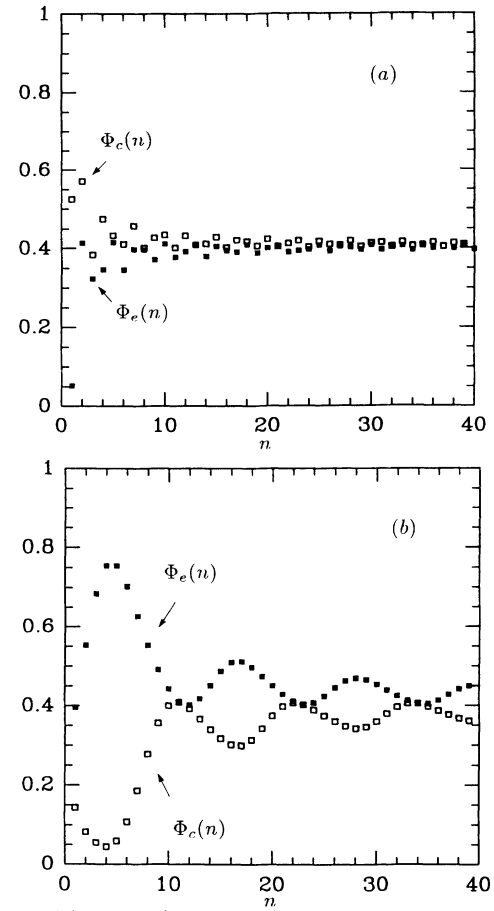

FIG. 15. The variation of convergence rate for finite-time average flux. The black dots correspond to escape, the white dots to capture, and the flux is per unit ϵA. For this example $(A_1,A_2)\equiv-(A,A)$, $A>0$, and (a) $(\omega_1,\omega_2)=(g,1)\omega_0$, $(\theta_{1_0},\theta_{2_0})=(\pi,0)$, (b) $(\omega_1,\omega_2)=(0.231,2.618)\omega_0$, and $(\theta_{1_0},\theta_{2_0})=(\frac{23}{22}\pi,\frac{3}{2}\pi)$.

effects cause the flux profile to dip below a linear increase from the lower to higher Φ. The single-frequency limit associated with the larger relative scaling factor thus corresponds to an absolute maximum of the average flux (the absolute minimum may or may not be at the other single-frequency limit, depending on the difference between the two relative scaling factors and the size of the dip due to interference effects). In this context, the best one can do is single-frequency forcing. In other contexts, however, including other aspects of flux, multiple-frequency forcing can enhance certain transport quantities. In particular, the variation of lobe areas gives one the freedom to vary instantaneous and finite-time average flux for a fixed infinite-time average. Relevant to the variation of finite-time average flux is the time scale for convergence to the infinite-time average. This time scale can be anywhere from relatively short to arbitrarily long

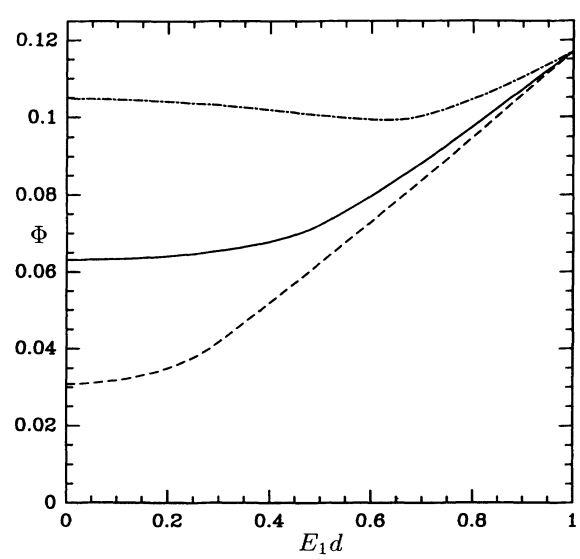

FIG. 16. Infinite-time average flux as a function of $E_1 d$, with $(E_1^2+E_2^2)d^2\equiv E^2d^2$. The frequency ω_1 is fixed at ω_0; the frequency ω_2 is $\frac{7}{3}\omega_0$ (dashed), ω_0/g (solid), and $\frac{10}{9}\omega_0$ (dashed-dotted). The flux is per unit $\epsilon(2\pi/a)Ed$, the horizontal axis is per unit Ed, and $\theta_{1_0}=\theta_{2_0}=0$.

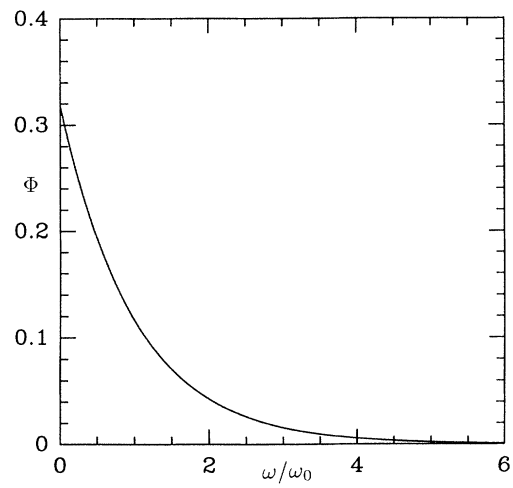

FIG. 17. The single-frequency infinite-time average flux as calculated by the Melnikov approximation (5.4). The flux is per unit $\epsilon(2\pi/a)Ed$.

(refer back to Fig. 15). We wish to stress the importance of the finite-time quantities, for, as we shall see, dissociation rates of course decay in time, so the dissociation process occurs over a finite time interval, and the infinite-time average flux may or may not have strong relevance to the problem at hand.

Just as the relative scaling function helps one understand the multiple-frequency case, so too does the flux associated with single-frequency forcing (see Fig. 17). The single-frequency infinite-time average flux given by (5.4) increases monotonically with decreasing forcing frequency ω, corresponding to infinite turnstile lobe area and maximal flux in the limit $\omega \to 0$. Such a result would seem to deserve an explanation. In comparison, MacKay and Meiss [7] obtain for a Coulomb potential a turnstile lobe area and flux which *both* diverge as $\omega \to 0$ for fixed ϵ. In their calculations they (along with Casati *et al.* [6]) consider dissociation of a prepared highly excited state ($n_0 = 66$), and they choose both ϵ and ω to depend on n_0; if one maintained this dependence as $n_0 \to \infty$ then *both* ϵ and ω would limit to zero, in such a way as to lead to divergent lobe area but zero flux. For the Morse potential we briefly discuss two cases of the limit $\omega \to 0$: (i) ϵ fixed and (ii) $\lim \epsilon \to 0$. For the case of ϵ fixed note from the Appendix [Eq. (A3)] that as $\omega \to 0$ the amplitude of oscillation of the p coordinate of τ_ϵ diverges, so that for sufficiently small ω the problem becomes no longer near-integrable. Figure 18 shows the turnstile lobe $L_{bu}(1)$ for four successively smaller values of ω. The lobe grows in area and spirals around R_b. There is no obvious reason why the lobe should not remain in a spiral as ω further decreases, and given that the stable manifold cannot intersect itself, $L_{bu}(1)$ would then be trapped entirely in R_b, allowing for two possibilities as $\omega \to 0$: either the area of the lobe and hence of R_b diverge, or the area of R_b will remain finite, forcing the turnstile lobe area to remain finite (this would not contradict Melnikov theory since we are not in the near-integrable regime). The plots sug-

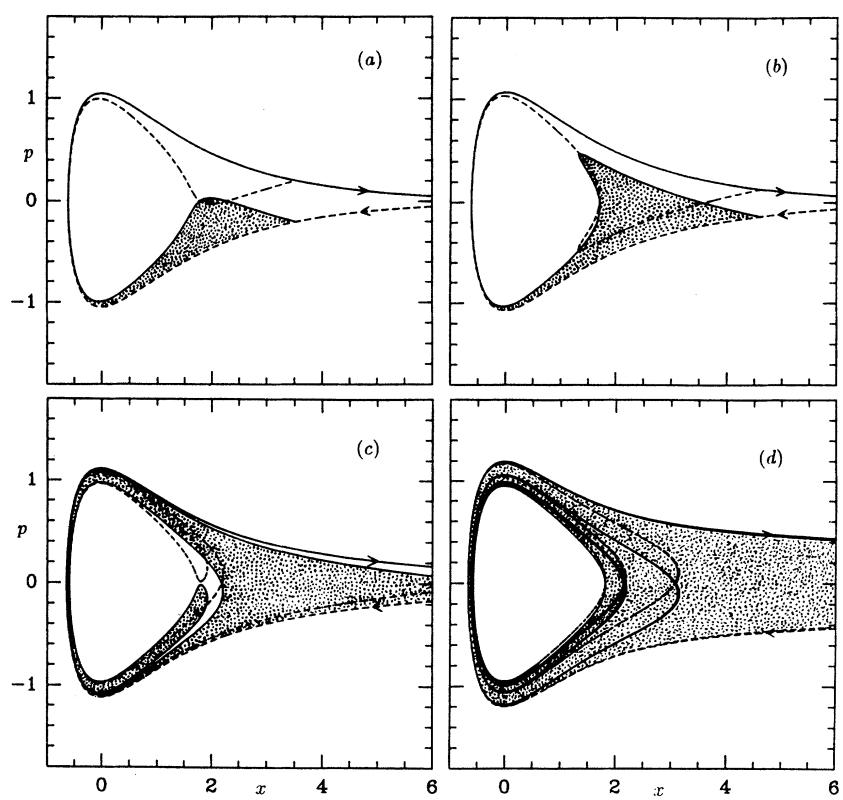

FIG. 18. The single-frequency lobe structure in $\Sigma^{\theta_1 = \pi}_0$ for four successively smaller forcing frequencies, with ϵEd fixed. The shaded lobe is the escape turnstile lobe $L_{bu}(1)$, and the white lobe is the image of the capture turnstile lobe $P_\epsilon(L_{ub}(1))$. For these examples $\epsilon Ed = 0.037\omega_0\sqrt{2mD_0}$, and (i) $\omega = 0.333\omega_0$, (ii) $\omega = 0.222\omega_0$, (iii) $\omega = 0.111\omega_0$, and (iv) $\omega = 0.0555\omega_0$.

gest that the areas will keep growing, though a much more intensive numerical study would be needed to assure this. Even if this were the case, however, one would of course not conclude from a maximal flux result that the aim for good dissociation rates is to make the forcing frequency arbitrarily small, for the followng reasons.

(i) That R_b grows with decreasing frequency implies that more and more of the phase space is eaten up by the bounded region.

(ii) One sees from Fig. 18 that as the frequency decreases a larger percentage of $L_{bu}(1)$ intersects with $P_\epsilon(L_{ub}(1))$, so that a larger percentage of phase-space trajectories escaping under the next iterate of P_ϵ were just captured at that time sample.

(iii) $L_{bu}(1)$ does not necessarily penetrate any better the inner level sets of the unperturbed Hamiltonian as ω decreases.

It is precisely issues such as these, such as the intersection of the turnstile lobes with other lobes and with level sets of the unperturbed Hamiltonian, that need to be dealt with for a complete study of dissociation rates, and we address these issues in the next two sections. We lastly remark here that for the case $\lim \epsilon \to 0$ the flux will fall to zero, and as long as ϵ/ω is kept sufficiently small the problem remains near-integrable (one would be interested in this situation for low-intensity microwave ionization or dissociation of highly excited states).

C. Dissociation rates

The main limitation of flux is that it involves phase space *areas* with no regard for the histories and initial conditions of phase-space trajectories within these areas. In the next two sections we study two basic phase-space transport questions relevant to molecular dissociation which addresses the history and location of phase-space trajectories. The question addressed in this section is: at time $t=(2\pi/\omega_2)n$, how many of the initially *bounded* points [i.e., those in $R_b(0)$ at $t=0$] have *escaped* [i.e., are in $R_u(n)$]? For $n>0$ the turnstile $L_{bu}(1;n)$ may in general contain points which were in $R_b(0)$ and $R_u(0)$ at $t=0$, so to answer this question one must know the history of the points in the turnstile lobe. Such a question is studied in the following language. At time $t=0$ let the regions $R_b(0)$ and $R_u(0)$ be covered *uniformly* with particles of species S_b and S_u, respectively, and let $\mathcal{T}_{bu}(n)$ [$\mathcal{T}_{ub}(n)$] denote the total amount of species S_b (S_u) contained in region $R_u(n)$ [$R_b(n)$] at $t=(2\pi/\omega_2)n$. Then for area-preserving sequences of maps

$$\mathcal{T}_{bu}(n+1)-\mathcal{T}_{bu}(n)=\mu_b(L_{bu}(1;n))-\mu_b(L_{ub}(1;n)) , \tag{5.5}$$

where $\mu_b(\ )$ denotes the area of the region within the parentheses that contains S_b. Equation (5.5) then quantifies a dissociation rate, and summing (5.5) over n [and using that $T_{bu}(0)=0$], one obtains an expression for $T_{bu}(n)$ for any n [of course, $T_{ub}(n)=T_{bu}(n)$, so we concentrate on $T_{bu}(n)$]. Solving Eq. (5.5) boils down to computing lobe *content* $\mu_b(L_{bu}(1;n))$ and $\mu_b(L_{ub}(1;n))$. We will discuss two approaches at solving for lobe content, one based on a Markov-model approach, applied to periodic forcing by MacKay, Meiss, Ott, and Percival [28,29] and extended here to quasiperiodic forcing, and one based on the study of the topology of lobe intersections with the bounded and unbounded regions and with other lobes, applied to periodic forcing by Rom-Kedar, Leonard, and Wiggins [26] and Rom-Kedar and Wiggins [35] and extended to quasiperiodic forcing by BLW [33,34].

The phase-space transport question studied in this section, that of an initial *uniform* distribution of points in phase space, is popular in chemical kinetics studies [15–21], but we point out that a study of an initial distribution that depends on energy levels would also seem worthwhile, and we will discuss this latter problem as well.

1. Markov models

The Markov-model approach provides an approximate answer to the first transport question in the context of periodic forcing, and has gained some popularity in the application to molecular dissociation. Its advantages are its conceptual simplicity and possible ease of implementation; its disadvantages are that it can lead to a poor approximation, one that can be even qualitatively incorrect and can miss basic features of transport. For a two-dimensional Poincaré map derived from time-periodic forcing, one has for the Poincaré section the same constructs as in the time slices of the quasiperiodic case, except that everything is independent of the sample time; hence, we use the same notation as in the quasiperiodic case, with the parameter n dropped. The Poincaré section is divided into two regions R_b and R_u, and for an elementary version of the Markov method often employed in chemical kinetics studies one further specifies for each of these regions the stochastic part that can participate in transport between R_u and R_b, denoted r_u and r_b, respectively. Thus r_b is the portion of R_b outside the outermost surviving KAM torus, minus the islands of stability, and calculating the area of this region *approximately* is not too difficult. One then assumes that once a lobe maps from one region to another, its contents instantaneously diffuse throughout the region it maps into. This rather unrealistic assumption allows one to determine lobe content in a simple manner. If we let $p\equiv\mu(L_{ub}(1))/\mu(r_b)$, i.e., p is the percentage of r_b occupied by the captured turnstile lobe, then *at the nth time sample*

$$\begin{aligned}&\mu_b(L_{bu}(1))=(1-p)^n\mu(L_{bu}(1)) ,\\ &\mu_b(L_{ub}(1))=0 ,\end{aligned} \tag{5.6}$$

and one finds

$$\mathcal{T}_{bu}(n)=[1-(1-p)^n]\mu(r_b) . \tag{5.7}$$

For a sequence of maps the Markov method generalizes in a simple manner: if we let $p_i\equiv\mu(L_{ub}(1;i))/\mu(r_b(i$

$+1)$), then the expression for $\mu_b(L_{bu}(1;n))$ becomes for $n \geq 1$

$$\mu_b(L_{bu}(1;n))=(1-p_0)(1-p_1)\cdots[1-p_{(n-1)}] \times\mu(L_{bu}(1;n)) \tag{5.8}$$

and one has

$$\mathcal{T}_{bu}(n)=\{1-(1-p_0)\cdots[1-p_{(n-1)}]\}\mu(r_b(n)) \ . \tag{5.9}$$

Since in general the p_i are different, one has for the sequence of maps added freedom to enhance or diminish aspects of transport over finite time scales. The previously mentioned influence of interference effects and relative scaling factors on the average lobe area are relevant to expressions (5.8) and (5.9), since the p_i are proportional to the turnstile lobe area. One must also consider the variation of $\mu(r_b(i))$ under the Markov model, but as should soon become clear, the dependence on $\mu(r_b(i))$ is a rather artificial consequence of the unrealistic approximation of infinitely fast diffusion. We lastly remark that for $p_0+p_1+\cdots+p_{(n-1)}=\text{const}$, the product $(1-p_0)\cdots(1-p_{(n-1)})$ is maximal in the limit $p_0=p_1=\cdots=p_{(n-1)}$ (this is just the simple result that the maximum volume of an n-sided box is associated with a cube), i.e., this product is maximal, given the constraint, in the single-frequency limit.

2. *The topology of lobe intersections*

An exact determination of lobe content, and hence an exact answer to the first transport question, necessitates a consideration of the topology of lobe intersections. Until now, we have discussed only the turnstile lobes $L_{bu}(1;n)$ [$L_{ub}(1;n)$], i.e., the lobes of the nth time slice that escape [are captured] between the nth and $(n+1)$th time slice; we now must consider other lobes $L_{bu}(m;n)$ [$L_{ub}(m;n)$], defined to be for $m \geq 1$ the lobes of the nth time slice which escape [are captured] between the $(n+m-1)$th and $(n+m)$th time slice (see Fig. 19). For quasiperiodic forcing, to find the true content of the turnstile lobes at $t=(2\pi/\omega_2)n$, one maps the lobes back to $t=0$ and sees how much of them are inside and outside $R_b(0)$,

$$\begin{aligned}\mu_b(L_{bu}(1;n))&\\ &=\{T_\epsilon^{-1}(\cdot;0)\circ\cdots\circ T_\epsilon^{-1}[L_{bu}(1;n);n-1]\}\cap R_b(0)\\ &=L_{bu}(1+n;0)\cap R_b(0)\ ,\\ \mu_b(L_{ub}(1;n))&=0\ ,\end{aligned} \tag{5.10}$$

where $T_\epsilon^{-1}(\cdot;n)$ denotes the map from the $(n+1)$th to the nth time slice. Since the stable manifold can never intersect itself, the only way for $L_{bu}(1+n;0)$, $n \geq 1$, to be outside $R_b(0)$ is for it to be inside the lobes $L_{ub}(m;0)$ for $1 \leq m \leq n$, as shown in Fig. 20 (note that it is due to the fact that the one-dimensional manifolds of each time slice are subject to the same geometrical constraints as those manifolds in the familiar case of periodic forcing that allows a straightforward extension of lobe intersection analysis to the quasiperiodic case). Hence one can

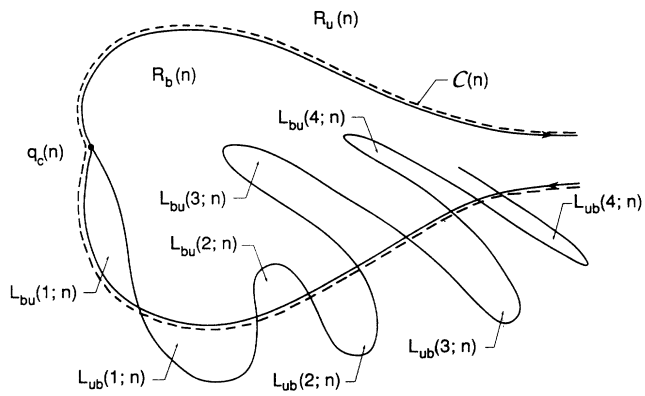

FIG. 19. Labeling the other lobes in the lobe structure. For simplicity of illustration we consider a case where there is only one lobe for each $L_{bu}(m;n)$, $L_{ub}(m;n)$, and we only portray the lobes for $m \geq 1$.

rewrite the first expression of (5.10) as

$$\mu_b(L_{bu}(1;n))=\mu(L_{bu}(1;n)) - \sum_{m=1}^{n}\mu(L_{bu}(1+n;0)\cap L_{ub}(m;0)) \tag{5.11}$$

(for $n=0$ replace the sum by zero). As n increases, the lobe intersections become exceedingly complicated, and the topology of the intersections is better appreciated by recognizing the approximate self-similar behavior of the preimages of the lobes as one evolves them backwards in time. These issues are discussed in BLW [40] in the context of two-dimensional maps, and we convey the essence of the situation for sequences of maps in Fig. 21. Once a lobe has completed one revolution around the bounded region, it begins to wrap around other turnstile lobes, as shown in Fig. 20 and highlighted by the shaded region in

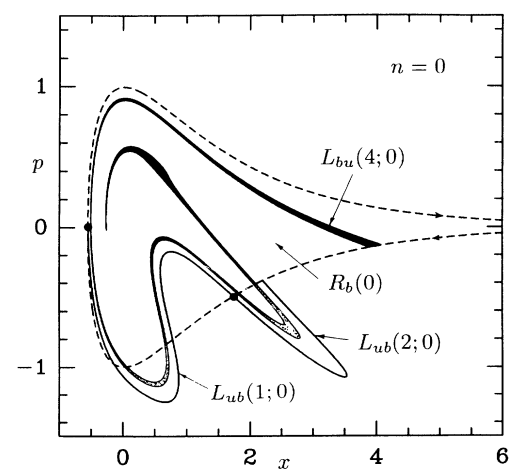

FIG. 20. Finding the content of a turnstile lobe. The parameters are the same here as in Figs. 9 and 12. In this particular example, we wish to determine the content of the escape turnstile lobe in the $n=3$ time slice, $L_{bu}(1;3)$. Hence we map the lobe back to the $n=0$ time slice [which gives the lobe $L_{bu}(4;0)$]: the black part of the lobe is in $R_b(0)$, and the speckled part is outside $R_b(0)$ and inside the lobes $L_{ub}(1;0)$ and $L_{ub}(2;0)$.

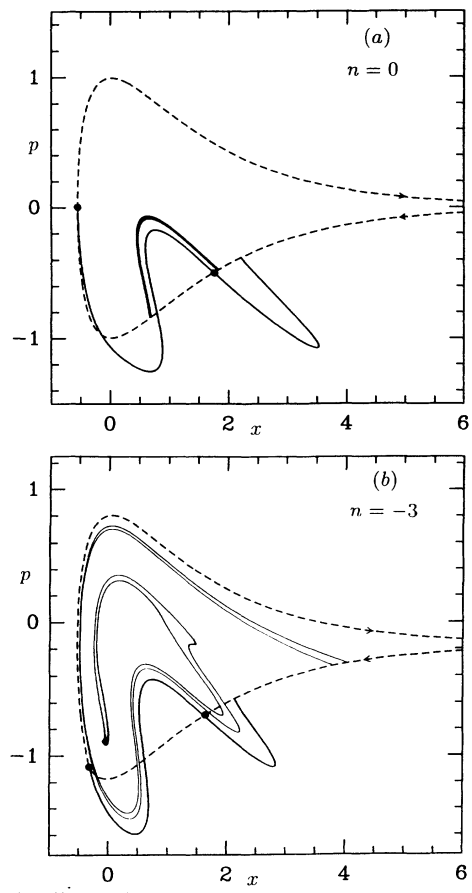

FIG. 21. Illustrating the approximate self-similar behavior as one maps a lobe backwards in time. In (a) we show a piece of the lobe $L_{bu}(4;0)$ in Fig. 20 that wraps around one of the $L_{bu}(1;0)$ lobes: we map this piece of lobe back another three periods to obtain (b). The resulting piece of lobe looks approximately like the boundary of the lobe $L_{bu}(1;3)$ mapped back three periods (compare with Fig. 20). This is an example where the approximate self-similarity is quite good: in general, since one has lobes of varying shape wrapping around one another, the approximate self-similarity is to be understood only very loosely.

Fig. 21(a). This shaded region then itself repeats the process of winding around the core under further evolution backwards in time, as shown in Fig. 21(b). One then understands the lobe intersections in terms of pieces of $L_{bu}(1;n)$ repeatedly revolving around the core under evolution backward in time until they intersect the turnstile $L_{ub}(1;\tilde{n})$, $\tilde{n}<n$: for each such piece the number of revolutions before the turnstile intersection can vary from 1 to ∞, and the period of each revolution can vary from some minimum number to ∞. One can construct a symbolic dynamics to describe the topology of these pieces [40], but we will not dwell on this here, our goal being merely to point out the complicated nature of the intersections, and yet the existence of a relatively simple framework with which to understand the topology of the intersections.

The intersection of lobes with $R_u(n)$ and $R_b(n)$, or equivalently with other lobes, provides the framework for exact computation of transport under quasiperiodic forcing, and we compare this framework with the approximate Markov model, and with periodic forcing. Our main interest is in the latter comparison, and we do not wish to digress too much with the former. A discussion of the deficiencies of the approximate Markov model has been given by Rom-Kedar and Wiggins [41] and Wiggins [23] (and is also pointed out by Zembekov [42]), and we only highlight here some of the results. Previous studies employing the Markov approximation show agreement with exact results only at short time scales [21,43]. Indeed any practical implementation of the Markov method entails exponential decay in transport rates, whereas the exact theory allows both exponential and power-law decay and the latter can indeed occur [36]. Even the short-time agreements can be viewed as rather accidental, for there is no reason to expect that the way lobes intersect one another bears any relation to the rather unrealistic process that assumes infinitely fast diffusion and disregards lobe intersections. In fact, we will soon mention in the context of quasiperiodic forcing a simple example where short-time agreement is not expected.

In comparing the exact transport theory for maps and sequences of maps, a central difference to recognize is the additional freedom in the latter case to enhance or diminish aspects of transport over finite time scales due to the variation of lobe areas. One can study this variation and exploit it to one's advantage by numerical simulation of the lobes. In Fig. 22 we show two simple examples that differ only in reversal of the sign of the amplitude for the first forcing frequency. In Fig. 22(a) the areas of the first six escape lobes are almost twice that of the average lobe areas, while the areas of the first six capture lobes are close to zero. Hence at short time scales the dissociation rates are almost twice as large as the infinite-time average flux. In Fig. 22(b) the situation is reversed: hence, after five time samples the content of the bounded region has changed significantly. A Markov-model approach would imply that the turnstile lobe $L_{bu}(1;5)$ contains a significant fraction of points that were not initially in the bounded region, but this is in fact not true since $L_{bu}(1;5)$ intersects with none of the captured lobes [on the scale shown it looks possible that $L_{bu}(1;5)$ just touches one of the capture lobes, but at greater resolution this is seen to not happen, which is consistent with the $n=0$ plot]. Despite the additional freedom of variation of lobe areas, one must also bear in mind that the average turnstile lobe area is maximal in a single-frequency limit, for lobe area does play a central role in phase space transport.

To numerically determine lobe content at any sample time $t=(2\pi/\omega_2)n$ for an initial uniform distribution in phase space, one could initialize the turnstile with a uniform distribution of points and then evolve the system backwards in time to $t=0$ and determine how many points are inside and outside $R_b(0)$. As mentioned earlier, one might also be interested in an initial distribution that depends on energy levels: for this one would employ the same procedure as above, except that at $t=0$ one would then weight the points in $R_b(0)$ according to the chosen distribution.

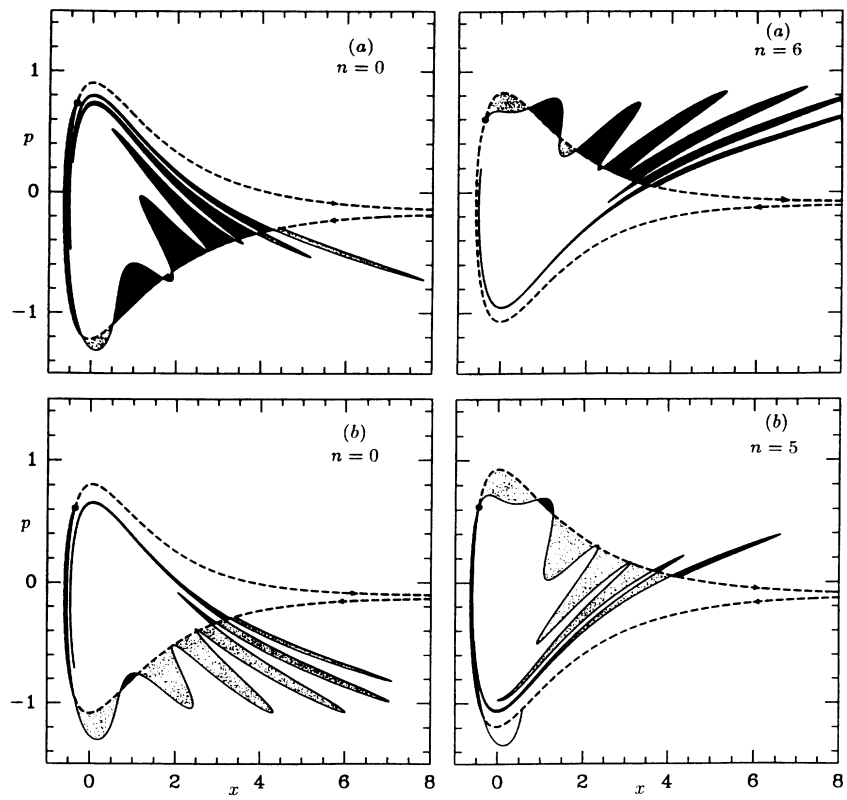

FIG. 22. Using variation of lobe areas to enhance or diminish finite-time escape or capture for a fixed infinite-time average flux. The parameters for (a) and (b) are identical to those in Fig. 13, except that ϵ is three times smaller here. The solid dot represents our choice of $q_c(n)$ for these examples, and in the $n=5$ sample for (b), $L_{bu}(1;5)$ is the thin black lobe that touches the dot.

D. Lobe penetration of energy levels and dissociation rates of a microcanonical ensemble

In addition to lobe *area* and lobe *content,* a third feature of dissociation to study in terms of phase-space transport is lobe *penetration,* meaning the ability of the lobes to penetrate along the action, or energy, coordinate. Indeed, there has been considerable interest in the ionization and dissociation of a system prepared in a particular quantum state [1–7,9,12,13], which in a classical context corresponds to the escape of an ensemble of points initialized on a particular level set of the unperturbed Hamiltonian. Previous studies have made no real connection to lobe dynamics within the homoclinic tangle; often there is discussion of such features as the presence of cantori and overlap of neighboring resonances [7,13], but these discussions are sometimes rather heuristic. As we have stressed, the sole mechanism for dissociation is the turnstiles of the homoclinic tangle, so any discussion of dissociation ultimately needs to be related to preimages of these turnstiles.

The transport equations, similar in spirit to Sec. V C, are easily written down. Let $\mathcal{L}_0$ denote the level set of interest of the unperturbed Hamiltonian, and $\Delta\mathcal{L}_0(n)$ denote the percentage of points initially on the level set that escape between the nth and $(n+1)$th time sample, then

$$\Delta\mathcal{L}_0(n)=\frac{\mu(L_{bu}(1+n;0)\cap\mathcal{L}_0)}{\mu(\mathcal{L}_0)}\ , \tag{5.12}$$

where $\mu(\ )$ denotes the number of points along the specified curve. One typically chooses the initial distribution on the level set to be uniform along the angle coordinate in action-angle space [which of course leads to a weighted distribution in (x,p) space]. Given this framework, one can divide the study of lobe intersections with the unperturbed level sets into three regimes, depending on the time scale $t=(2\pi/\omega_2)n$.

(i) Short time scale—small n. For small n the shapes of the lobes $L_{bu}(1+n;0)$ are not very convoluted and their thickness normal to the unperturbed separatrix is well approximated by the Melnikov expression (3.2). In the small-n regime we can identify two aspects of the lobes that affect penetration.

(a) The Melnikov function provides a measure of *relative penetration,* as described below. Let

$$q_\epsilon^{s,u}(-s,\theta_1,\theta_{2_0};\nu)$$
$$=q_{\epsilon=0}(-s)+\epsilon\frac{\partial q_\epsilon^{s,u}}{\partial\epsilon}(-s,\theta_1,\theta_{2_0};\nu)|_{\epsilon=0}+O(\epsilon^2)$$

denote the (x,p) component of a point on $W^s(\tau_\epsilon)$ and $W^u(\tau_\epsilon)$, respectively, where $q_{\epsilon=0}(-s)$ is the (x,p) component of a point on the unperturbed separatrix. Then

$$H(q_\epsilon^u)-H(q_\epsilon^s)=H(q_{\epsilon=0})+\epsilon DH(q_{\epsilon=0})\cdot\frac{\partial q_\epsilon^u}{\partial\epsilon}\bigg|_{\epsilon=0}+O(\epsilon^2)-H(q_{\epsilon=0})-\epsilon DH(q_{\epsilon=0})\cdot\frac{\partial q_\epsilon^s}{\partial\epsilon}\bigg|_{\epsilon=0}-O(\epsilon^2)$$
$$=\epsilon DH(q_{\epsilon=0})\cdot\left[\frac{\partial q_\epsilon^u}{\partial\epsilon}-\frac{\partial q_\epsilon^s}{\partial\epsilon}\right]\bigg|_{\epsilon=0}+O(\epsilon^2)\ . \tag{5.13}$$

By definition [22,32] the first-order term in the last line of (5.13) is $\epsilon M(s,\theta_1,\theta_{2_0};\nu)$. Hence

$$H(q_\epsilon^u(-s,\theta_1,\theta_{2_0};\nu))-H(q_\epsilon^s(-s,\theta_1,\theta_{2_0};\nu))$$
$$=\epsilon M(s,\theta_1,\theta_{2_0};\nu)+O(\epsilon^2)\ . \tag{5.14}$$

The interpretation is thus that ϵM gives the first-order measure of how the lobe boundaries span the energy levels of the *unperturbed* Hamiltonian. In the small-n regime, then, the previously discussed influence of relative scaling factors and interference effects on the Melnikov function have relevance on the lobes' ability to span the unperturbed energy levels. Recall from Sec. V B that if for any pair of frequencies (ω_1,ω_2) we vary the amplitudes (E_1,E_2) with $E_1^2+E_2^2$ fixed, then $\langle|\epsilon M|\rangle_s$ is maximal in the single-frequency limit corresponding to the larger relative scaling factor [where $\langle\ \rangle_s$ denotes the average over $s\in(-\infty,\infty)$]. For the small-n regime we are interested in a finite s interval, so that, though $\langle|\epsilon M|\rangle_s$ can have an influence in this regime, it is also balanced by the added freedom of two-frequency forcing to enhance or diminish $|\epsilon M|$ over a finite s interval for a fixed $\langle|\epsilon M|\rangle_s$. Additionally relevant to lobe penetration is the *maximum* value of $|\epsilon M|$: though interference effects cause $\langle|\epsilon M|\rangle_s$ to dip *below* a linear increase as the (E_1,E_2) weighting is varied from the lower to higher relative scaling factor (refer back to Fig. 16), $|\epsilon M|_{\max}$ will be *raised* above a linear increase, so that the span of the unperturbed energy levels can be maximal in the two-frequency case (see Fig. 23).

(b) In addition to a measure of the range of unperturbed energy levels spanned by the lobes, i.e., the *relative* penetration, one is also interested in the *absolute* penetration of energy levels, i.e., in how the lobes penetrate any particular level set, which is affected not only by lobe width along the energy coordinate, but also the previously mentioned net oscillation and "breathing" of the lobe structure. A measure of the net oscillation in the p coordinate is given by the expression for τ_ϵ [see Eq. (A4) in the Appendix]: the amplitudes of the p_ϵ oscillation are $\epsilon dE_i/\omega_i$ for the ω_i component. The breathing of the lobe structure is more difficult to study and, as previously explained, one will typically need to resort to numerical simulation of the lobe structure. We wish to stress the importance of the breathing and oscillations of the lobe structure, for it can have a significant effect on dissociation: for example, it can allow portions of a high-quantum-number bounded level set to initially be already *outside* $R_b(0)$. Though not explicitly mentioned in the next two regimes, it should be understood that the net breathing and oscillations are relevant there too.

(ii) Intermediate time scale—medium n. In this regime n is, on the one hand, large enough that the lobes $L_{bu}(1+n;0)$ wind around $R_b(0)$, wrapping around other escape lobes and intersecting other capture lobes (recall the earlier discussion of the approximate self-similar behavior of the lobes to help make sense of this intermediate regime); however, n is still small enough that the penetration process has not yet approached saturation. It is in this intermediate regime that explicit numerical simulation of the lobes is most worthwhile, for the analytical tools and constructs applicable to the limiting regimes of small n and large n (to be discussed next) have only partial relevance here. The Melnikov function, useful in the small-n regime, offers no accounting for how the lobes further penetrate the energy levels by repeatedly winding around the core and wrapping around other lobes. Additionally, until the penetration process approaches saturation, the large-n constructs we will mention (such as the outermost surviving KAM-type torus) may have little relevance. The constructs of both limiting regimes will have *some* relevance, though: the intermediate-n lobes wrap around the small-n lobes, and hence the penetration of these small-n lobes does affect the penetration of the intermediate-n lobes. Conversely, the large-n constructs, such as the outermost surviving KAM-type torus, will serve as an inner barrier that limits penetration. The single- and two-frequency comparisons will thus be influenced by the comparisons in the two limiting regimes, but a true comparison will necessitate numerical simulations on a case by case basis.

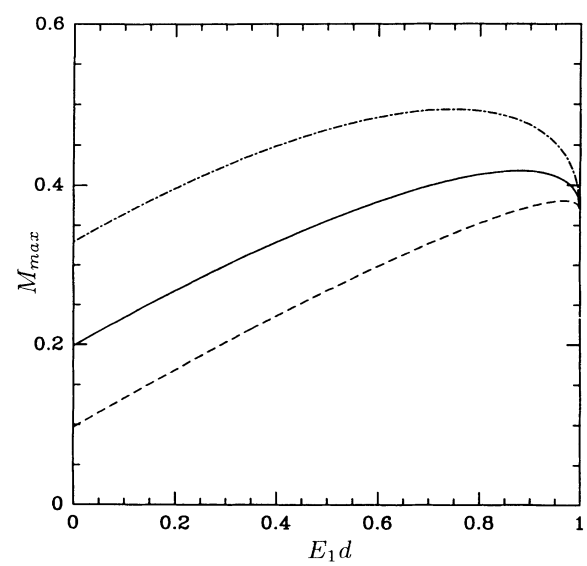

FIG. 23. Plot of $M_{\max}$ as a function of $E_1 d$, with $(E_1^2+E_2^2)d^2\equiv E^2d^2$. The parameters are identical to those of Fig. 16. $M_{\max}$ is per unit $(2\pi/a)Ed$, and the horizontal axis is per unit Ed.

(iii) Long time scale—large n. For large enough n the ability of the lobes to penetrate the unperturbed energy level saturates. In principle one could study dissociation in terms of lobe dynamics until saturation, but to do this would be quite computer intensive (a large-n calculation might be interesting nevertheless). Other constructs are useful in this regime and have been employed in the single-frequency case: in particular, the outermost surviving KAM-type torus provides a phase-space boundary that encloses a region in phase space whose points remain bounded for all time. Hence the escape lobes can never penetrate past this torus, which thus acts as a barrier to lobe penetration. In this respect there is interest in the overlap of neighboring resonances [13], for such an overlap disallows a surviving KAM-type torus between the two resonances, and thus can be used as a tool for estimating the location of the outermost surviving KAM-type torus. We remark parenthetically that Arnold [44] indicates how original KAM theory extends to quasiperiodically forced one-degree-of-freedom Hamiltonian systems.

Goggin and Milonni [12,13] study one-frequency and two-frequency dissociation *thresholds* for an ensemble of points on a level set corresponding to the ground state of the Morse oscillator: they numerically compute the forcing intensity needed to dissociate 5% of the level set once the dissociation process has been saturated. They provide numerical evidence that two-frequency forcing has a *lower* threshold intensity, and argue that this lowering is a consequence of the additional resonances created by the additional forcing frequency, which facilitates resonance overlap and hence dissociation. We add two qualifications to their results. First, the sole numerical comparison for dissociation they offer keeps one of the frequencies in the two-frequency problem fixed at what is almost the "best" available frequency (i.e., lowest single-frequency threshold intensity), so that much of the comparison amounts to one between a relatively poor single-frequency forcing (high-threshold intensity) and a combination of one good and one poor frequency in the two-frequency problem, a somewhat unfair comparison. Nevertheless, their comparison offers *some* evidence of a lower two-frequency threshold, though not so striking as their visual comparison suggests at first glance. Second, the presence of additional resonances alone does not ensure enhanced resonance overlap, for if one has, for example, twice as many resonances at half the width, it is not obvious that one has gained anything. Since forcing intensity is proportional to the sum of the *squares* of the electric fields, however, it is possible to have in the two-frequency problem at least twice as many resonances at *more* than half the width for the same intensity as the single-frequency problem. It is thus plausible that with the ideal frequency combinations one will have enhanced resonance overlap, and a lower threshold intensity.

After distinguishing between the above three regimes, we point out that much of the previous studies of ionization and dissociation focus on a fairly specific situation: the *threshold regime,* where the forcing intensity is at the threshold where ionization and dissociation just begin. This corresponds to the situation where the lobes $L_{bu}(1+n;0)$ intersect the level set only in the saturation regime (large n). Another interesting situation that deserves study is what we will call the *post-threshold* regime, where the forcing intensity is larger than the threshold intensity for the level set concerned, and the escape lobes $L_{bu}(1+n;0)$ thus play a role in dissociation for small and medium values of n. As should be clear from our discussion, the threshold and post-threshold regimes can have qualitatively different behavior and necessitate different methods of investigation. We end this section with three remarks to highlight these differences and some of the issues in the post-threshold regime.

(i) Constructs relevant to the threshold regime, such as cantori, resonance overlap, and the outermost surviving KAM-type torus, may have little relevance to the post-threshold regime. For example, in the case where the concerned level set intersects the turnstiles, it should be clear that issues such as resonance overlap can have little relevance.

(ii) The penetration dependence on forcing frequency in the threshold and post-threshold regime may differ. In the threshold regime, the frequency of the concerned level set can have particular relevance; for example Goggin and Milonni [13] offer evidence that for one-frequency forcing it is best to force near this frequency (i.e., one obtains the lowest threshold intensity near the level-set frequency). A reasonable argument for this phenomenon is that as one increases the forcing intensity to find the threshold regime, and hence moves the outermost surviving KAM torus to smaller and smaller action values, having a nice thick 1:1 resonance at the concerned level set awaiting the incoming KAM torus will facilitate resonance overlap and hence facilitate moving the KAM torus inside the level set. For the post-threshold regime, however, the relevant neighboring resonances will have already overlapped and the level-set frequency may have less relevance.

(iii) Consider a particular scenario as an example of the more varied questions one can address in the post-threshold regime (also of interest for comparing with quantum-mechanical calculations). Suppose we force at some fixed intensity and some fixed frequency tuned, say, to the ground-state dissociation energy, and ask how dissociation rates change for an initial distribution of points on a high-quantum-number level set as we increase the quantum number, i.e., move closer to the separatrix. On the one hand, for a fixed forcing intensity and frequency the turnstile lobes are fixed, so that as the level set of interest approaches the separatrix its intersection with the turnstile can approach a constant length, so that the numerator of (5.12) approaches a constant. However, the arclength and period of the level set increases to infinity, so that the transition rate falls to zero.

E. Chaos

We close with a comment on the chaotic nature of the dynamics associated with quasiperiodic forcing, or equivalently, with sequences of maps, and the ability to detect a chaotic response to quasiperiodic forcing. It has of course been widely appreciated for a long time that the

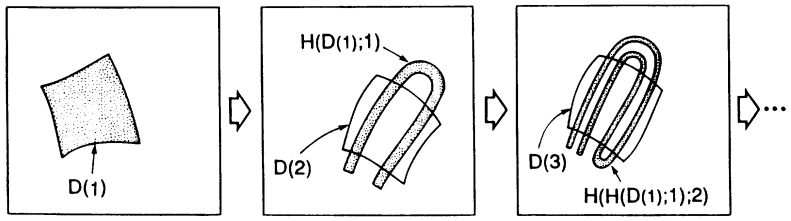

FIG. 24. A traveling horseshoe map sequence.

chaotic nature of the dynamics in homoclinic and heteroclinic tangles of two-dimensional *maps* is understood in terms of the presence of a Smale horseshoe map. How does one understand chaos for *sequences of maps?* As described rigorously in BLW [33,34], and as discussed heuristically here, chaos is understood in terms of the presence of a *traveling horseshoe map sequence* $\{H(\cdot;n);n\in Z\}$ (see Fig. 24). The sequence consists of a bi-infinite sequence of domains

$$\{\ldots,D(-n),\ldots,D(-1),D(0),D(1),\ldots,D(n),\ldots\}$$

such that $H(D(n);n)$ intersects $D(n+1)$ in a horseshoelike fashion. The result is chaotic dynamics relative to a *time-dependent* Cantor set of points.

VI. CONCLUDING REMARKS

Invariant manifolds offer a basic framework for studying classes of nonintegrable systems. For a periodically or quasiperiodically forced nonlinear oscillator such as the Morse oscillator, the stable and unstable manifolds of the corresponding Poincaré map's homoclinic tangle provide a precise criterion for the partial barriers between bounded and unbounded motion and for the sole mechanism of transport across these partial barriers, the turnstiles. Having identified these phase-space structures one can study a variety of transition rates between bounded and unbounded motion, and hence perform a classical study of molecular dissociation.

Addressing the quasiperiodically forced Morse oscillator necessitates a basic extension past the ubiquitous single-frequency case, for one must generalize from two-dimensional *maps* to *sequences of two-dimensional maps,* or equivalently to a three-dimensional Poincaré map acting on a sequence of two-dimensional phase slices. As we have seen, however, the constructs associated with iterates of a two-dimensional map are fairly robust: a fixed set of partial barriers and turnstiles generalizes to a sequence of partial barriers and turnstiles, and the Smale horseshoe map generalizes to a traveling horseshoe map sequence. A generalized Melnikov function and a double-phase-slice sampling method provide the analytical and computational tools for studying two-frequency dissociation in the context of sequences of maps and comparing with the single-frequency case. On the one hand, infinite-time average flux is seen to be maximal in the single-frequency limit associated with the larger relative scaling factor; however, lobe penetration of the level sets of the unperturbed Hamiltonian can be maximal in the two-frequency case. Additionally, the variation of lobe areas in the two-frequency problem gives one added freedom to enhance or diminish aspects of transport over finite time scales for a fixed infinite-time average flux.

Melnikov theory and the results based on this theory are valid in the near-integrable regime; however, in practice fairly large perturbations are allowed (refer, for example, to Fig. 5). More significantly, we stress that the basic framework used here, i.e., the use of invariant manifolds to partition phase space, identify partial barriers and turnstiles, and study molecular dissociation via phase-space transport and lobe dynamics, does not require near-integrability.

For simplicity of discussion, we have focused on two-frequency forcing; however, a similar analysis applies to multiple-frequency systems with more than two forcing frequencies, and indeed to more complicated forcing time dependences than quasiperiodic, as explained in BLW [33,34].

ACKNOWLEDGMENTS

This material is based upon work supported by the National Science Foundation and the Office of Naval Research.

APPENDIX

We include here a few mathematical details about the quasiperiodically forced Morse oscillator.

(i) The expression for an orbit on the unperturbed separatrix $(x_h(t-s),p_h(t-s))$ is solved by setting $H=D_0$, where H is the unperturbed Hamiltonian, and using $\dot{x}=p/m$ to obtain

$$\dot{x}=\pm\sqrt{2D_0/m}\,(2e^{-ax}-e^{-2ax})^{1/2}\ .$$

One can integrate this to obtain x and hence $p=m\dot{x}$

$$\begin{aligned} x_h(t-s)&=\frac{1}{a}\ln\left[\frac{1+[\omega_0(t-s)]^2}{2}\right],\\ p_h(t-s)&=2\sqrt{2mD_0}\,\frac{\omega_0(t-s)}{1+[\omega_0(t-s)]^2}\ , \end{aligned} \tag{A1}$$

where $\omega_0\equiv a\sqrt{2D_0/m}$.

(ii) The expression for the invariant 1-torus τ_ϵ in $\Sigma^{\theta_{2_0}}$ is solved by setting $z=1/x$ and studying the Morse system at $z=0$,

$$\begin{aligned} \dot{z}&=0\ ,\\ \dot{p}&=\epsilon d[E_1\cos(\omega_1 t+\theta_{1_0})+E_2\cos(\omega_2 t+\theta_{2_0})]\ , \end{aligned} \tag{A2}$$

which is solved by

$$z(t)=0\ ,$$
$$p(t)=\epsilon d\left[\frac{E_1}{\omega_1}\sin(\omega_1 t+\theta_{1_0})+\frac{E_2}{\omega_2}\sin(\omega_2 t+\theta_{2_0})\right]\ . \tag{A3}$$

The expression for τ_ϵ is thus given by

$$(x_\epsilon(\theta_1),p_\epsilon(\theta_1))$$
$$=\left[\lim x\to\infty,\epsilon d\left[\frac{E_1}{\omega_1}\sin(\theta_1)+\frac{E_2}{\omega_2}\sin(\theta_{2_0})\right]\right]\ . \tag{A4}$$

(iii) *Calculation of the Melnikov function.* From (3.1) $M(s,\theta_1,\theta_2;\nu)=I_1+I_2$ where

$$I_i=\frac{E_i d}{m}\int_{-\infty}^{\infty}p_h(t)\cos[\omega_i t+(\omega_i s+\theta_i)]dt\ ,\quad i=1,2\ . \tag{A5}$$

Using (A1) and that $p_h(t)$ is odd in t

$$I_i=-\frac{4E_i d}{a}\sin(\omega_i s+\theta_i)\times\int_0^\infty\frac{\omega_0 t}{1+(\omega_0 t)^2}\sin(\omega_i t)d(\omega_0 t)\ ,\quad i=1,2\ . \tag{A6}$$

Solving the integral gives

$$I_i=-\frac{2\pi}{a}E_i d e^{-\omega_i/\omega_0}\sin(\omega_i s+\theta_i)\ ,\quad i=1,2\ . \tag{A7}$$

Note that (A7) is valid for $\omega_i>0$; for $\omega_i=0$ the integrand in (A6) is identically zero and hence I_i vanishes. The Melnikov function is thus discontinuous at $\omega_i=0$ due to the nonvanishing of the Melnikov amplitudes in the limit $\omega_i\to 0$. This nonvanishing is due to the fact that $p_h(t)\sim 1/(\omega_0 t)$ for large $|t|$.

(iv) *The Melnikov approximation of manifold separation.* If we assume differentiable stable and unstable manifolds we obtain by Taylor expanding in ϵ

$$d(s,\theta_1,\theta_{2_0};\nu,\epsilon)=\epsilon\frac{\Delta^u(0,s,\theta_1,\theta_{2_0};\nu)-\Delta^s(0,s,\theta_1,\theta_{2_0};\nu)}{\|DH(q_h(-s))\|}+O(\epsilon^2) \tag{A8}$$

where $q_h(-s)\equiv(x_h(-s),p_h(-s))$ and

$$\Delta^{s,u}(t,s,\theta_1,\theta_2;\nu)\equiv DH(q_h(t-s))\cdot\frac{\partial q_\epsilon^{s,u}(t,s,\theta_1,\theta_2;\nu)}{\partial\epsilon}\bigg|_{\epsilon=0}\ ,$$

with $q_\epsilon^{s,u}$ the (x,p) component of an orbit on the perturbed stable and unstable manifold, respectively, in the full autonomous system phase space. Employing the standard procedure of deriving and solving a linear differential equation for $\Delta^{s,u}$ in t [22,32], one obtains

$$\Delta^u(0,s,\theta_1,\theta_{2_0};\nu)-\Delta^s(0,s,\theta_1,\theta_{2_0};\nu)$$
$$=M(s,\theta_1,\theta_{2_0};\nu)+\lim_{t\to-\infty}\Delta^u(t,s,\theta_1,\theta_{2_0};\nu)-\lim_{t\to\infty}\Delta^s(t,s,\theta_1,\theta_{2_0};\nu)\ . \tag{A9}$$

The nonhyperbolicity and infinite radius of τ_ϵ means that the convergence of the Melnikov integral and the vanishing of the two limits is not guaranteed without additional analysis. The Melnikov integral was explicitly shown to converge in (iii). The two limits in (A9) vanish as long as

$$\lim_{|t|\to\infty}DH(q_h(t-s))=0\ ,$$

and

$$\lim_{t\to\infty,-\infty}\frac{\partial q_\epsilon^{s,u}(t,s,\theta_1,\theta_{2_0};\nu)}{\partial\epsilon}$$

is bounded. The first condition is easily seen to hold, and it should be noted that it does not require hyperbolicity, only that τ_ϵ be of saddle-type stability. The second condition is seen to be satisfied for the component $p_\epsilon^{s,u}$ due to (A3). Both $x_{\epsilon>0}^{s,u}$ and $x_{\epsilon=0}^{s,u}$ limit to infinity as $t\to\infty,-\infty$, but their difference is

$$x_{\epsilon>0}^{s,u}-x_{\epsilon=0}^{s,u}=\frac{1}{m}\int(p_{\epsilon>0}^{s,u}-p_{\epsilon=0}^{s,u})dt\ , \tag{A10}$$

and hence the bounded oscillations of p in (A3) imply bounded oscillations in x at infinity. The constant of integration in (A10) may become unbounded in the concerned limit, but since

$$\frac{\partial H}{\partial x}[q_h(t-s)]\sim 1/(t-s)^2$$

for large $|t-s|$, all we really need is for $\partial x_\epsilon^{s,u}(t,s,\theta_1,\theta_{2_0};\nu)/\partial\epsilon$, or equivalently $x_{\epsilon>0}^{s,u}(t,s,\theta_1,\theta_{2_0};\nu)-x_{\epsilon=0}^{s,u}(t-s)$, not to diverge faster than t^2 with increasing $|t|$, which is guaranteed by the fact that for large $|t|$, $x_{\epsilon=0}^{s,u}(t-s)\sim\ln|t-s|$ and $|\dot{x}_{\epsilon>0}^{s,u}(t,s,\theta_1,\theta_{2_0};\nu)|$ decays to bounded oscillations with zero mean as t approaches $\infty,-\infty$ asymptotically (indeed, numerical studies show that the x component of points on the perturbed stable and unstable manifolds grows logarithmically for large $|t|$ with increasing and decreasing time, respectively, which would imply that the constant of integration in (A10) remains bounded anyway). We remark that the excellent agreement in Fig. 5 between the exact manifold separation and the Melnikov approximation (3.2) can be taken as confirmation that both limits in (A9) indeed vanish, and that the assumption of differentiable stable and unstable manifolds is valid.

[1] J. G. Leopold and I. C. Percival, Phys. Rev. Lett. **41**, 944 (1978).
[2] J. G. Leopold and I. C. Percival, J. Phys. B **12**, 709 (1979).
[3] R. V. Jensen, Phys. Rev. A **30**, 386 (1984); in *Proceedings of the Oji International Seminar on Highly Excited States of Atoms and Molecules,* edited by S. Kano and M. Matsuzawa (Fuji-Yoshida, Japan, 1986), p. 149.
[4] J. G. Leopold and D. Richards, J. Phys. B **18**, 3369 (1985).
[5] J. N. Bardsley and M. J. Comella, J. Phys. B **19**, L565 (1986).
[6] G. Casati, B. V. Chirikov, D. L. Shepelyansky, and I. Guarneri, Phys. Rev. Lett. **57**, 823 (1986).
[7] R. S. MacKay and J. D. Meiss, Phys. Rev. A **37**, 4702 (1988).
[8] R. B. Walker and R. K. Preston, J. Chem. Phys. **67**, 2017 (1977).
[9] D. W. Noid and J. R. Stine, Chem. Phys. Lett. **65**, 153 (1979).
[10] G. C. Lie and J. M. Yuan, J. Chem. Phys. **84**, 5486 (1986).
[11] M. Tung and J. M. Yuan, Phys. Rev. A **36**, 4463 (1987).
[12] M. E. Goggin and P. W. Milonni, Phys. Rev. A **37**, 796 (1988).
[13] M. E. Goggin and P. W. Milonni, Phys. Rev. A **38**, 5174 (1988).
[14] Z. M. Lu, J. F. Heagy, M. Vallières, and J. M. Yuan, Phys. Rev. A **43**, 1118 (1991).
[15] M. J. Davis, J. Chem. Phys. **83**, 1016 (1985).
[16] M. J. Davis and S. K. Gray, J. Chem. Phys. **84**, 5389 (1986).
[17] S. K. Gray, S. A. Rice, and M. J. Davis, J. Phys. Chem. **90**, 3470 (1986).
[18] M. J. Davis, J. Chem. Phys. **86**, 3978 (1986).
[19] R. T. Skodjie and M. J. Davis, J. Chem. Phys. **88**, 2429 (1988).
[20] P. Gaspard and S. A. Rice, J. Phys. Chem. **93**, 6947 (1989).
[21] R.E. Gillilan and G. S. Ezra, J. Chem. Phys. **94**, 2648 (1991).
[22] J. Guckenheimer and P. Holmes, *Nonlinear Oscillations, Dynamical Systems, and Bifurcations of Vector Fields* (Springer-Verlag, New York, 1983).
[23] S. Wiggins, *Chaotic Transport in Dynamical Systems* (Springer-Verlag, New York, 1991).
[24] F. M. A. Salam and S. S. Sastry, IEEE Trans. Circuits Syst. **32**, 784 (1985).
[25] K. Hockett and P. Holmes, Ergod. Theory Dynam. Syst. **6**, 205 (1986).
[26] V. Rom-Kedar, A. Leonard, and S. Wiggins, J. Fluid Mech. **214**, 347 (1990).
[27] I. S. Kang and L. G. Leal, J. Fluid Mech. **218**, 41 (1990).
[28] R. S. MacKay, J. D. Meiss, and I. C. Percival, Physica D **13**, 55 (1984).
[29] J. D. Meiss and E. Ott, Physica D **20**, 387 (1986).
[30] L Moorman, E. J. Galvez, B. E. Sauer, A. Mortazawi-M., K. A. H. van Leeuwen, G. v. Oppen, and P. M. Koch, Phys. Rev. Lett. **61**, 771 (1988).
[31] S. Wiggins, Physica D **44**, 471 (1990).
[32] S. Wiggins, *Global Bifurcations and Chaos—Analytical Methods* (Springer-Verlag, New York, 1988).
[33] D. Beigie, A. Leonard, and S. Wiggins, Nonlinearity **4**, 775 (1991).
[34] D. Beigie, A. Leonard, and S. Wiggins, in *Nonlinear Phenomena in Atmospheric and Oceanic Sciences (IMA Volumes in Mathematics and its Applications),* edited by G. F. Carnevale and R. Pierrehumbert (Springer-Verlag, New York, in press), Vol. 40.
[35] V. Rom-Kedar and S. Wiggins, Arch. Ration. Mech. Anal. **109**, 239 (1990).
[36] B. Bruhn, Ann. Phys. (Leipzig) **46**, 367 (1989).
[37] D. Bensimon and L. P. Kadanoff, Physica D **13**, 82 (1984).
[38] R. S. MacKay and J. D. Meiss, J. Phys. A **19**, L225 (1986).
[39] R. S. MacKay, J. D. Meiss, and I. C. Percival, Physica D **27**, 1 (1987).
[40] D. Beigie, A. Leonard, and S. Wiggins, Phys. Fluids A **3**, 1039 (1991).
[41] V. Rom-Kedar and S. Wiggins, Physica D **51**, 248 (1991).
[42] A. A. Zembekov, Phys. Rev. A **42**, 7163 (1990).
[43] R. Camassa and S. Wiggins, Phys. Rev. A **43**, 774 (1991).
[44] V. I. Arnold, Russ. Mat. Surveys **18**, 85 (1963).

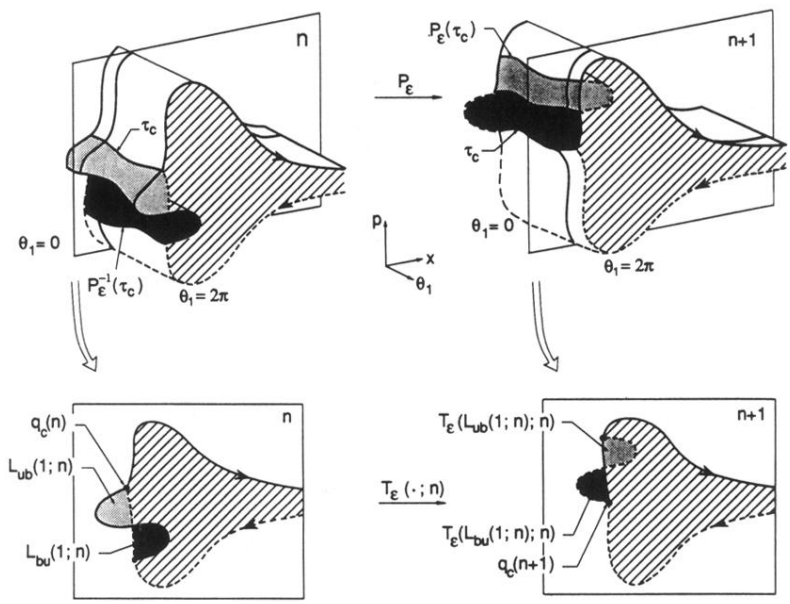

FIG. 11. The turnstiles as the sole mechanism for transport between the bounded and unbounded regions.

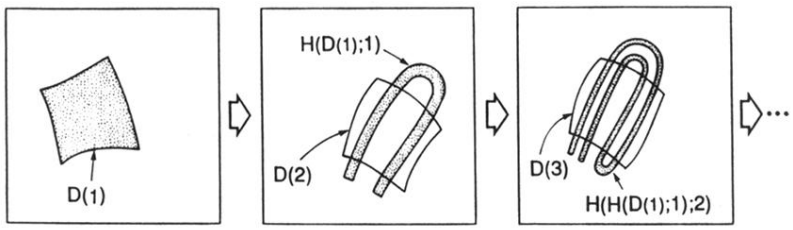

FIG. 24. A traveling horseshoe map sequence.